Chapter 8
Micro/Nano Electrochemical Sensors for Ion Sensing

Jiawei Tu, Hao Wan, and Ping Wang

Abstract The developments in micro/nano electrochemical sensors have large impact on ion sensing research. Significant advances in the fabrications of micro/nano electrochemical sensors are being persistently made. Micro/nano electrochemical sensors play a very significant role in electrochemistry for ion sensing. Compared to conventional electrochemical sensors, micro/nano sensors exhibit nonlinear diffusion with higher sensitivity, higher current density, faster mass transfer, and higher signal-to-noise ratio. Hence, micro/nano electrochemical sensor is widely applied for various ion sensings. The theory of electrochemical sensors for ion sensing, which contains potentiometric sensors, voltammetric sensors, microelectrode array, and LAPS, is described in this chapter. Also a self-designed integrated sensor with microelectrode array (MEA) and light-addressable potentiometric sensor (LAPS) for heavy-metal ion and pH detection is introduced, and its fabrication and the characterization of MEA and LAPS are described. Electrochemical measurements have shown numerous advantages for trace heavy-metal detection, including rapid analysis, good selectivity, andsensitivity. Therefore, some applications in environment and food analysis related to the electrochemical analysis of ion sensing are discussed in this chapter.

Keywords Ion sensing • Microelectrode array (MEA) • Light-addressable potentiometric sensor (LAPS)

8.1 Introduction

Micro/nano electrochemical sensors have been applied in various fields, in which ion sensing in water environment has received extensive concerns for researchers. Among all these ions in water, heavy metals are especially concerned due to the

J. Tu • H. Wan • P. Wang (✉)
Biosensor National Special Laboratory, Department of Biomedical Engineering, Zhejiang University, Hangzhou, China
e-mail: cnpwang@zju.edu.cn

P. Wang et al. (eds.), *Micro/Nano Cell and Molecular Sensors*,
DOI 10.1007/978-981-10-1658-5_8

properties of high toxicity, bioaccumulation, and nonbiodegradability. Extensive heavy metals such as zinc, copper, cadmium, lead, mercury, and chromium can result in severe hazards to the ecosystem and human health. For instance, excessive intake of lead can lead to neurological, neurobehavioral, hematological, and renal diseases, especially potentially harmful to neurodevelopment of infants and children [1, 2]. Copper poisoning may cause hepatitis, liver cirrhosis, jaundice, and hemolytic crisis [3, 4]. Mercury poisoning could lead to damage of the brain, kidneys, and lungs, which resulted in the Minamata Bay tragedy in the 1950s. Thus, heavy-metal ion sensing is of great significance and urgency for human and the environment. Among all approaches for heavy-metal analysis such as atomic absorption spectroscopy (AAS) and inductively coupled plasma mass spectroscopy (ICP-MS), electrochemistry demonstrates its superior merits in terms of sensitivity, detection of limit, and low cost. Besides, heavy-metal sensing is easily implemented with simultaneous detection of several heavy-metal ions. Micro/nano electrochemical sensors play a very significant role in electrochemistry for ion sensing. Compared to conventional electrochemical sensors, micro/nano sensors exhibit nonlinear diffusion with higher sensitivity, higher current density, faster mass transfer, and higher signal-to-noise ratio. Hence, micro/nano electrochemical sensor is widely applied for various ion sensings.

8.2 Theory of Electrochemical Sensors for Ion Sensing

Based on different parameters measured in electrochemical analysis, electrochemical sensors mainly embrace three different sensors, potentiometric sensor, voltammetric sensor, and conductometric sensor. In this chapter, we mainly discuss potentiometric sensor and voltammetric sensor.

8.2.1 Potentiometric Sensors

In potentiometry, a potential is measured between two electrodes under the conditions of no current flow. The measured potential may then be used to determine the analytical quantity of interest, generally the concentration of some component of the solution. The potential that develops in the electrochemical cell is the result of the free energy change that would occur if the chemical phenomena were to proceed until the equilibrium condition has been satisfied.

The largest group among potentiometric sensors is represented by ion-selective electrodes (ISEs), the oldest and most widely used among them being a pH-sensitive glass electrode. Different approaches of potentiometric electronic tongues and taste sensors have been demonstrated. They have in common that they all measure the potential over a charged membrane. These membranes can be of different materials, which provide enough selectivity to different classes of chemical substances. Electronic tongues have, thus, been described based on an

Fig. 8.1 ISEs and the measuring system (Reproduced with permission from [5]. Copyright 2015 Elsevier B.V.)

array of chalcogenide glass sensors, including conventional electrodes such as chloride-, sodium- and potassium-selective sensors, combined with a pattern-recognition routine. The photograph of ISEs' array and the measuring system in the group of Andrey Legin, St. Petersburg University (Russia), is shown in Fig. 8.1. The chalcogenide sensors show cross sensitivity, which has been preferably used for measurement of metal ions in river water, and suggested or environmental and process-monitoring purposes. This type of electronic tongues has also been combined with PVC membranes for testing of beverages.

Potentiometric ion and chemical sensors based on field-effect devices form another group of transducers that can be easily miniaturized and are fabricated by means of microelectronic technology. Among them the most studied are the ion-sensitive field-effect transistors (ISFETs) with different ion-selective membranes (often also called chemically sensitive field-effect transistors or Chem-FETs). ISFETs with bare gate insulator (silicon oxide, silicon nitride, aluminum oxide, etc.) show intrinsic pH sensitivity due to electrochemical equilibrium between the protonated oxide surface and protons in the solution. To obtain sensitivity to other ions, a polymeric membrane containing some ionophore may be deposited.

Light-addressable potentiometric sensor (LAPS) is a semiconductor-based device with an electrolyte-insulator-semiconductor (EIS) structure, which is similar to ISFET in function. A DC bias voltage is applied to LAPS, so that a depletion layer appears at the insulator-semiconductor interface. When a modulated light irradiates LAPS from the front or back side, an AC photocurrent inside the depletion layer could be induced as a measured signal. The amplitude of the photocurrent is sensitive to the surface potential and thus LAPS is able to detect the potential variation caused by an electrochemical even. Therefore, in principle,

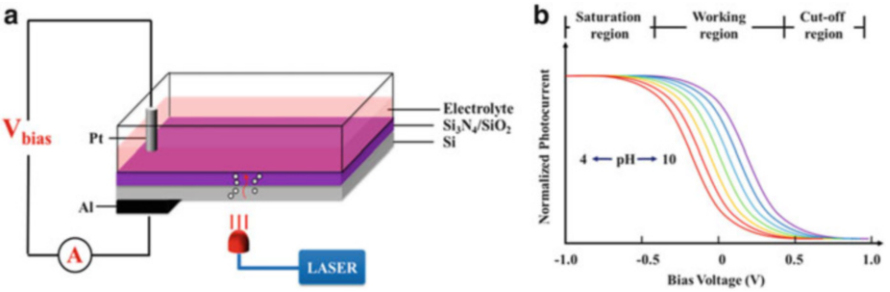

Fig. 8.2 (**a**) Working principle of the LAPS. (**b**) Characteristic I–V curve of N-type LAPS (Reproduced with permission from [6]. Copyright 2015 Science Press, Beijing and Springer Science + Business Media Dordrecht)

any electrochemical reaction that results in the change of surface potential can be detected by LAPS, including the ionic change and redox effect, shown in Fig. 8.2a. By modifying the individual sensitive region with the polymer membrane or chalcogenide glass membrane which contains specific receptor molecules, relevant cations could be detected simultaneously. Most of the solid-state-based thin-film sensors suffer from an insufficient selectivity. Compared to the inorganic membrane, the organic one can overcome the problem with reasonable good selectivity. The characteristic I–V curve of N-type LAPS is shown in Fig. 8.2b.

8.2.2 Voltammetric Sensors

Voltammetry, in which a current is measured at a fixed potential, is a very powerful and often used technique in analytical chemistry. Depending on the potential applied and type of working electrode, redox active compounds are either oxidized or reduced at the working electrode, giving rise to a current. The sensitivity of voltammetric methods is often very high. The selectivity is, however, in many cases poor, since all compounds in a measured solution that are electrochemically active below the applied potential will contribute to the measured current. Different ways to surmount this is, e.g., to cover the working electrode with a gas permeable membrane, only letting gases pass through, or to use pulse voltammetry. Voltammetry appears to have several advantages; the technique has been extensively used in analytical chemistry due to features such as its very high sensitivity, versatility, simplicity, and robustness. Besides, voltammetry offers a widespread number of different analytical possibilities, including cyclic, stripping, and pulse voltammetry. Depending on the technique, various kinds or aspects of information can be obtained from the measured solution. Normally, redox active species are being measured at a fixed potential, but by using, e.g., pulse voltammetry, studies of transient responses when Helmholtz layers are formed also give information concerning diffusion coefficients of charged species. Further information is also

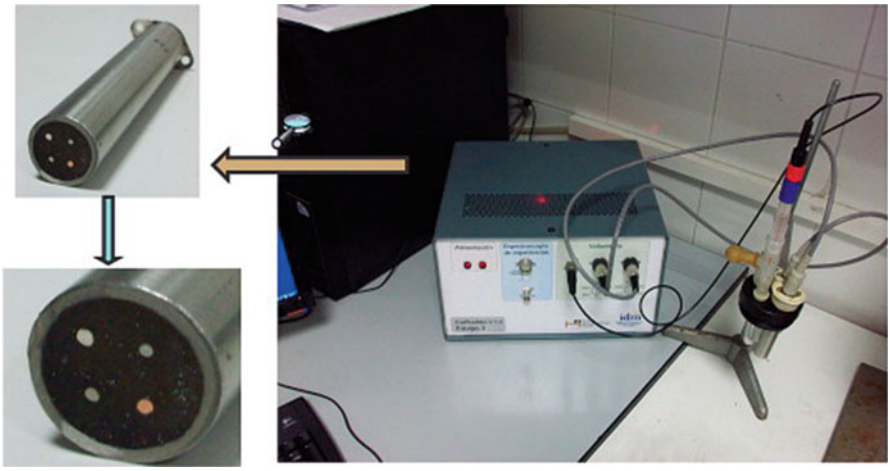

Fig. 8.3 A developed voltammetric electronic tongue for water quality monitoring (Reproduced with permission from [7]. Copyright 2013 by the authors; licensee MDPI, Basel, Switzerland)

obtainable by the use of different types of metals for the working electrodes. Different metal electrodes can be used together with voltammetric measurements to classify different liquids. Still, the voltammograms contain a large amount of information, and to extract this information, multivariate calibration methods have been shown to be rather efficient. A developed voltammetric electronic tongue for water quality monitoring is shown in Fig. 8.3.

In our group, we mainly use voltammetric sensors for heavy-metal analysis, specifically stripping voltammetry. The principle of stripping voltammetry includes three steps: heavy-metal reduction, equilibrium, and reoxidation. First, heavy-metal ions are reduced on the surface of working electrodes under a constant potential. In this step, stirring is generally used to further enhance the mass transfer rate. The equilibrium step ensures an equilibrium reaction in samples without stirring and reduction. Then a positive scanning potential is applied on the working electrode in order to reoxidate the heavy metal, and oxidation current is recorded in this step. Thus, voltammograms are obtained and stripping peaks are linearly correlated with concentrations of heavy metals, by which quantification of heavy metals in a sample is implemented. Specific detection is implemented based on the characteristic oxidation potential. In this deposition step, heavy-metal ions are reduced on a very small working electrode, thus resulting in the enrichment of heavy metals. The detection of limit is about 10^{-8}–10^{-9} mol/L for trace heavy-metal analysis. And in stripping voltammetry, several factors can affect the performance in heavy-metal analysis:

1. Deposition potential. Deposition potential is generally optimized due to its impact on the reduction rate. Besides, more positive deposition potential can lead to unstable reduction reaction, affecting the reproducibility of stripping

analysis. More negative deposition potential may lead to hydrogen evolution and reduction of other heavy-metal ions, by which interferences may be introduced.
2. Deposition time. In a certain range of deposition time, the stripping current of heavy metals is linearly correlated with deposition time. Longer deposition time can lead to the saturation of the working electrode due to the small effective area of working electrodes, which affects the linear detection range in heavy-metal analysis. Short deposition time leads to a decrease of sensitivity and current response in stripping analysis.
3. Scanning rate. Generally, the stripping peak current is linearly correlated with the scanning rate, while faster scanning rate may introduce larger background noise and charging current.
4. Stirring rate. The stirring rate is the essential factor to the reproducibility in heavy-metal analysis and faster stirring rate can also result in higher current response. In our study, differential pulse stripping voltammetry (DPSV) and square wave stripping voltammetry (SWSV) are mainly utilized in our research, which can effectively decrease the background current and increase the signal-to-noise ratio.

8.2.3 Characterizations of Micro/Nano sensors

Well-designed micro/nano sensors usually have the following characteristics: large mass transfer rate and current density, low time constant and IR voltage drop, low charging current, and high signal-to-noise ratio. These characteristics can be described by the corresponding radius diffusion which is dependent on the shape of sensors. Furthermore, the characteristics of microelectrode array are quite more complex than a single electrode.

8.2.3.1 Radius Diffusion

For conventional macroelectrodes, when the active concentration on the surface of working electrode is 0, the relationship between current response and time could be described using Cottrell equation:

$$i(t) = \frac{zFAD^{1/2}C}{\pi^{1/2}t^{1/2}} \tag{8.1}$$

Under this condition, the active substances on the surface of working electrodes diffuse vertical to the surface due to the macro-size of working electrodes shown in Fig. 8.4a. This phenomenon is called linear diffusion. When the size of working electrodes decreases to the size of diffusion layer, mass transfer occurs according to

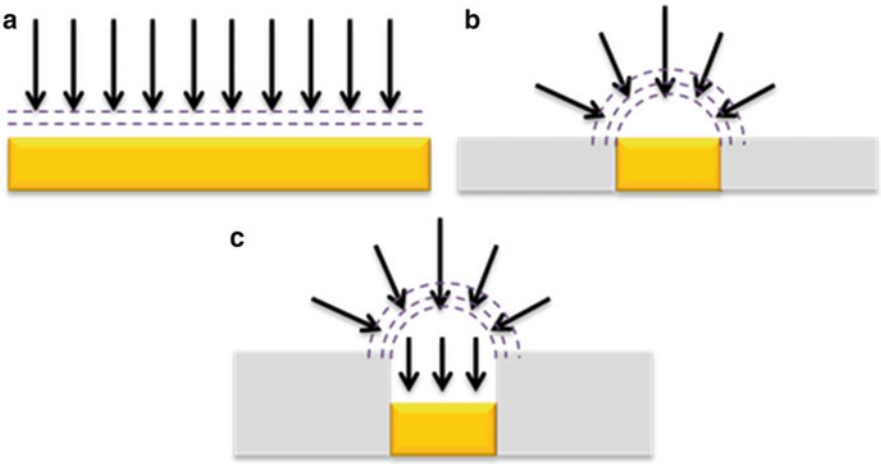

Fig. 8.4 Different shapes of working electrodes. (**a**) Linear diffusion, the active substances on the surface of working electrodes diffuse vertical to the surface; (**b**) radius diffusion, the active substances diffuse around the surface; (**c**) radius diffusion in recessed electrodes, the active substances diffuse upon the surface similar to radius diffusion

the radius direction on the surface, called radius diffusion. In this situation, the Cottrell equation is revised:

$$i(t) = \frac{zFAD^{1/2}C}{\pi^{1/2}t^{1/2}} + \frac{4zFADC}{\pi r} \tag{8.2}$$

where the first item represents the current produced by linear diffusion and the current decreases with the increasing of time. The second item represents the current produced by radius diffusion, which is not related with time, shown in Fig. 8.4b. In electrochemical analysis, the current produced by linear diffusion decreases to 0 after reaction for a period of time. Then the total current is mainly produced by radius diffusion and the current is called steady-state current, which is not changed with time variation. The steady-state current is only related to the radius of micro/nano electrodes. For instance, when using micro/nano disk electrodes for electrochemical analysis, the steady-state current could be described in the equation:

$$i_d = 4zFDCr \tag{8.3}$$

In some cases, recessed micro/nano electrodes are applied in electrochemical analysis since an insulation layer is deposited on the working electrode region shown in Fig. 8.4c. In this situation, the equation is revised in which L represents

the depth of the recessed electrodes and r represents the radius of working electrodes:

$$i_d = \frac{4zFDCr}{\left(\frac{4L}{\pi r} + 1\right)} \tag{8.4}$$

8.2.3.2 Large Mass Transfer Rate and Current Density

According to Eq. 8.4, the steady-state current is linearly correlated with the radius of micro/nano electrodes. Since the size of micro/nano electrodes is usually microscale or nanoscale, the produced current is very low between 10^{-9} and 10^{-12} A. The current density is inversely proportional to the radius of the electrodes, which means larger current density is produced with smaller size. Hence, very large current density could be acquired with micro/nano electrodes compared to conventional macroelectrodes.

The mass transfer rate on the surface of working electrodes can be expressed by Eq. 8.5, where D represents the diffusion coefficient of different active substances and δ is the thickness of diffusion layer. Mass transfer rate represents the spread rate of active substances in the diffusion. For macroelectrodes, the mass transfer rate decreases with the increasing of time due to the linear diffusion as expressed in Eq. 8.6. For micro/nano electrodes, the mass transfer rate is expressed in Eq. 8.7 with the radius diffusion on the surface of working electrodes. In these cases, the mass transfer rate keeps steady and is not related with the time variation, only dependent on the diffusion coefficient and radius of micro/nano electrodes. Compared to macroelectrodes, micro/nano electrodes have large mass transfer rate, which ensures the steady state in a very short time. Hence, instead of stirring and rotating in macroelectrode application, micro/nano electrodes present extraordinary performance in electrochemical analysis without any stirring:

$$M = \frac{D}{\delta} \tag{8.5}$$

$$M = \frac{D^{1/2}}{\pi^{1/2} t^{1/2}} \tag{8.6}$$

$$M = \frac{4D}{\pi r} \tag{8.7}$$

8.2.3.3 Low Time Constant and IR Voltage Drop

In electrochemical analysis, the charging current is produced in the electric double layer on the surface of working electrodes during step-potential scanning. The

relationship between the charging current and time is expressed in Eq. 8.1. As shown in the equation, the charging current is exponential to the capacitance of electric double layer and related with the resistance of the working cell. The time constant is expressed as $\tau = RC_s$, indicating that the charging current decays rapidly with a small time constant. The capacitance of electric double layer is proportional to the area of working electrodes. Hence, the time constant is very small due to the microscale or nanoscale size of micro/nano electrodes, which means the charging current could decrease to 0 in a very short time. For instance, in a micro-disk electrode with radius of 2.5 μm, the charging current of electric double layer could decrease to 1 % in only 12 ns.

In the electrochemical reaction, when the step of micro- and nanoelectrode potential sweep, this will result in the charging current in the electric double layer electrode surface. Charging current versus time is shown in Eq. 8.1. By the above equation, the charging current exponentially changes with the electric double-layer capacitor and is closely related to the internal resistance of the cell. The time constant $\tau = \mathrm{RCs}$, the smaller the time constant, the faster the charging current decays. Since the electric double-layer capacitor Cs is directly proportional to the electrode area, and the area of micro/nano electrode is very small, a very small time constant, the charging current decays to near zero within a very short time [8]. For example, the charging current of the electric double layer decays to 99 % need only 12 ns for a radius 2.5 μm micro-disk electrode. Therefore, the scan rate can be very fast during step-potential scanning, without worrying about the introduction of excessive charging current component because of the fast scan rate. Compared to conventional large electrode, micro/nano electrodes are more suitable for a variety of transient electrochemical analysis methods, such as differential pulse stripping voltammetry and square wave stripping voltammetry. Micro/nano electrodes also greatly reduce the time required for voltammetry in fast potential sweep.

i_R drop is due to the pressure drop in the internal resistance of the cell caused by the current flowing through, so that the voltage actually applied to the working electrode is different from the expected value. Since the current real-time changes in the process of electrochemical reaction, the working electrode voltage varies with time and greatly affects the accuracy of electrochemical analysis. The introduction of a three-electrode system is to solve the problem of i_R drop by using the reference electrode to provide a constant potential for the working electrode. For micro/nano electrodes, the current strength is typically 10^{-9}–10^{-12} A, so i_R drop is very small. For conventional electrodes, the i_R drop is generally up to 5–10 mV. The i_R drop of the micro/nano electrodes is typically several μV or less and is negligible for electrochemical analysis. Therefore, we could use two-electrode system when using a micro/nano electrode as the working electrode. It also simplifies instrument configuration and maintenance procedures without the reference electrode. In addition, the microelectrodes can be applied in the electrochemical analysis of a high-impedance state media.

8.2.3.4 Low Charging Current, High Signal-to-Noise Ratio

The charging current is shown in Eq. 8.1. The time constant of micro/nano electrodes is small, so the charging current is small. The current in the electrochemical reaction is composed of Faraday current and charging current. Faraday current will decay with $t^{1/2}$, and the charging current will decay exponentially with time. So the ratio of the Faraday current and charging current is very large in the step scan. In the case study of micro-disk electrode, Faraday current is independent of time under steady-state conditions. In a single-sweep voltammetry, the SNR of the electrode is:

$$\eta = \frac{i_f}{i_c} = \frac{4zFDC}{\pi C_s r v} \tag{8.8}$$

By the above equation, the SNR of the electrode increases with the decreasing radius. For conventional electrodes, according to the Randles-Sevcik equation, the SNR is:

$$\eta = 0.446\left(\frac{\mathrm{zFD}}{RT}\right)^{1/2}\frac{zFC}{v^{1/2}C_s} \tag{8.9}$$

The radio of micro/nano electrode's SNR and conventional electrode's SNR is:

$$\xi = \frac{\eta_m}{\eta_n} = \frac{(DRT)^{1/2}}{0.1114\pi r(zFv)^{1/2}} \tag{8.10}$$

For an example of radius 5 μm disk microelectrode, when the scan rate is 20 mV/s, $\xi = 20$. That means micro/nano electrode's SNR is 20 times the conventional electrode's SNR under the same conditions. Micro/nano electrodes have a very high SNR [8]; it helps to reduce the detection limit and can be used for qualitative and quantitative analysis of trace substances.

8.2.3.5 Microelectrode Array Characteristics

Single micro/nano electrode's current response strength is very small. The direct detection of the detection circuit has a very high demand. Thus, microelectrode array which is composed of a plurality of micro/nano electrodes is used in actual electrochemical analysis. Microelectrode array has the characteristic of a single electrode, but also has the following features:

1. Current additivity. In microelectrode array, micro/nano electrodes are connected in parallel; when there is no interaction between the electrodes, the total current is the sum of a plurality of micro/nano electrodes.
2. i_R drop and the time constant do not change. In microelectrode array, the total current is the sum of a plurality of micro/nano electrodes. Current increases n

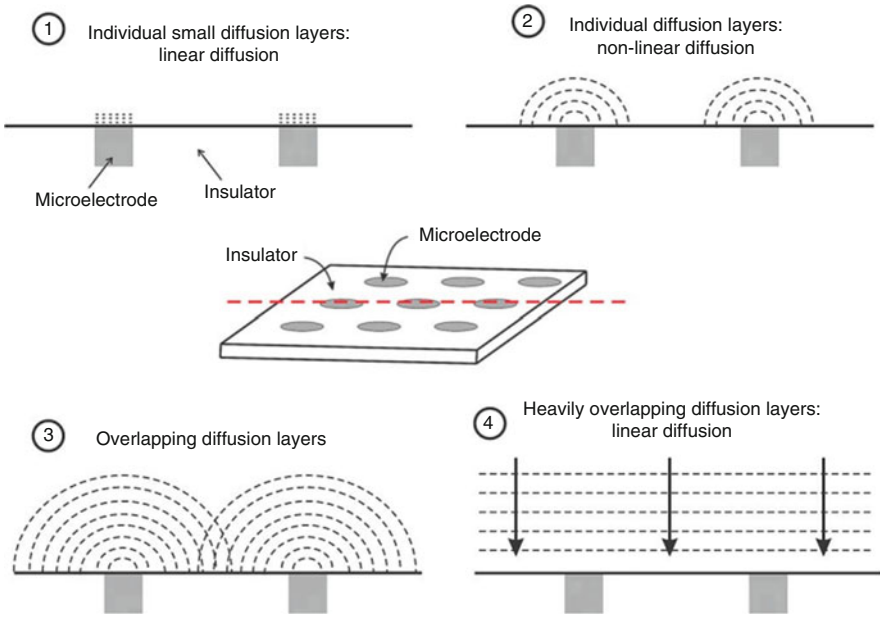

Fig. 8.5 Diffusion characteristics of microelectrode array under different circumstances (Reproduced with permission from [10]. Copyright 2005 Elsevier B.V.)

times, and the resistance is reduced to one n-th. Therefore, i_R drop remains unchanged. Similarly, the total capacitor increases n times because of electrodes are parallel. So the time constant RCs is also unchanged.

3. The shielding effect. Diffusion layer appeared on each micro/nano electrode surface because of substance diffusion. When the pitch of micro/nano electrodes is too close, it will lead to a diffusion layer between the electrode overlap. The response current of the electrode decreases, resulting in shielding effect.

How to avoid the shielding effect of the microelectrode array is an important research to study the characteristics of microelectrode array. The shielding effect is related to the size of micro/nano electrodes, electrode spacing, and diffusion layer thickness. Figure 8.5 shows the diffusion characteristics of microelectrode array under different circumstances [9]. In picture 1, diffusion layer thickness is much smaller than the size of the electrodes so that the linear diffusion appeared on the electrode surface; when the size of the electrode is reduced to the diffusion layer thickness in picture 2, nonlinear diffusion appeared on the electrode surface with the characteristics of low time constant and high SNR. No overlap between the diffusion layer since the distance between the electrodes is far. The distance between electrodes is too close in picture 3, resulting in the shielding effect because of diffusion layer overlap. The distance between electrodes is close but far less than the thickness of the diffusion layer in picture 4, and the diffusion layer has heavily overlap, resulting in linear diffusion instead of nonlinear diffusion. Thus, in the

design of micro/nano electrode array, we should ensure that the small size of the electrodes and the distance between electrodes are sufficiently large that a single micro/nano electrode has nonlinear dispersion characteristics.

8.3 Electrochemical Ion Sensors and Measurement

In this part, we introduce a self-designed integrated sensor with microelectrode array (MEA) and LAPS for heavy-metal ion and pH detection. Au-MEA was utilized for quantitative determination of zinc, lead, and copper, while hydrogen sensitive LAPS was deployed for pH detection in the meanwhile. Due to the significant influence of pH variation to heavy-metal detection, pH value provided by LAPS can be used as the guidance in heavy-metal analysis and further data calibration can be introduced to enhance the accuracy of sensors for heavy-metal quantification.

8.3.1 Fabrication of the Hybrid Sensor

The detailed process for the hybrid chemical sensor fabrication is shown in Fig. 8.6. A 430 μm N-type single crystal silicon wafer was used as the substrate. After RCA clean, LAPS sensing area on the back was etched to 100 μm thick for the enhancement of light permeability, while the rest was protected by photoresist. Thus, the induced alternating photocurrent by illuminating with a modulated light from the back would increase accordingly. Thermal oxidation was employed afterward to form a 50 nm SiO_2 layer in dry oxygen. A 100 nm Si_3N_4 layer was deposited by plasma enhanced chemical vapor deposition (PECVD) upon the SiO_2 layer. The notch, the 100 μm thick area of wafer, and the layers of SiO_2 and Si_3N_4 formed a preliminary structure of LAPS.

A 500 nm SiO_2 layer was deposited by PECVD to eliminate adverse effects on LAPS during the fabrication of MEA and form the insulation between the silicon and MEA. The metal layer was composed of gold and titanium, by which the Ti layer enhanced the adhesion between Au and the substrate. The sensing area of MEA was retained with photoresist while the rest areas were etched. An additional 800 nm Si_3N_4 layer was deposited for the insulation of signal conducting, while the Si_3N_4 layer upon the sensing sites of MEA was etched by photolithographic masks. An aluminum layer was evaporated for Ohmic contact by thermal evaporation. The fabrication of hybrid sensor array was accomplished and utilized for further electrochemical analysis.

The structure of the hybrid sensor fabricated is shown in Fig. 8.7. Section 1 in Fig. 8.7a represents the LAPS sensing areas for pH detection. The sensing area of

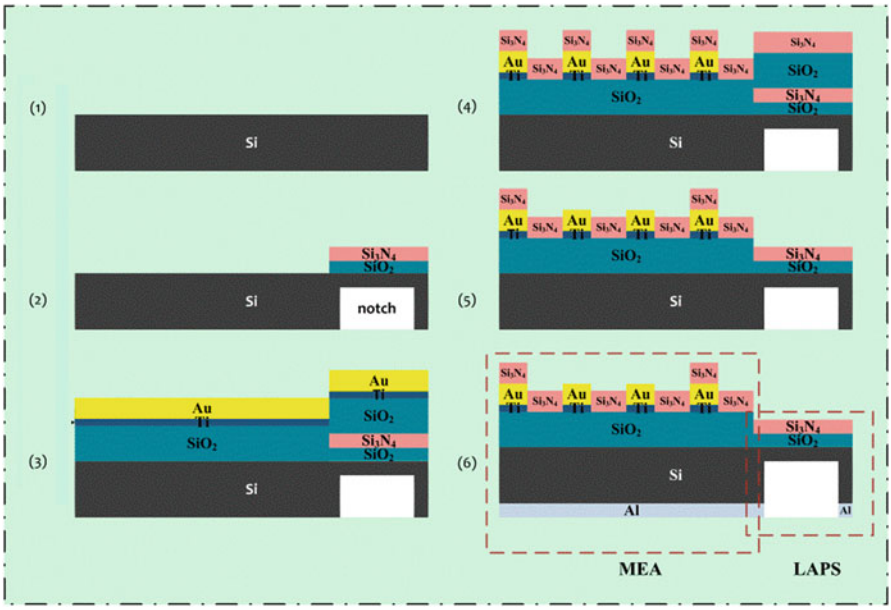

Fig. 8.6 The detailed process for the hybrid chemical sensor fabrication (Reproduced with permission from [11]. Copyright 2013 Elsevier B.V.)

each LAPS was 3.5 × 3.5 mm, while the modulated light (LED) was fixed in the notch behind each sensing surface to engender photocurrent. Two different MEA patterns were fabricated on the sensor in which one was micro-disk electrode array (MEAs 2–5) with the same gold substrate in Fig. 8.7c and the other was consisted of individual disk microelectrodes (MEAs 6–7) in Fig. 8.7d. MEAs 2–3 have a diameter of 50 μm and 30 μm, respectively, while 4 × 4 microelectrodes with interelectrode spacing of 200 μm were fabricated on individual sensing area. By contrast, MEAs 4–5 were consisted of 5 × 5 microelectrodes. MEAs 6–7 were in the same parameters with MEAs 2–3 except for the different patterns. Thus, characterizations of microelectrodes with different sizes, numbers, and patterns can be investigated. The circumambient gold electrodes (Sect. 8) of MEA and LAPS were deployed as the counter electrode. The packaged hybrid sensor is shown in Fig. 8.7b for practical electrochemical analysis.

The scheme of the hybrid sensor is shown in Fig. 8.8. MEA, LAPS, and counter electrode (CE) are integrated on the sensor, and signals are acquired through corresponding bonding pads by signal acquisition module. External reference electrode (RE) immersed in saturated KCl was used, thus constituting a three-electrode system with the working electrode and CE on the sensor. Light source for LAPS was placed at the back of etched LAPS sensing area with light modulation.

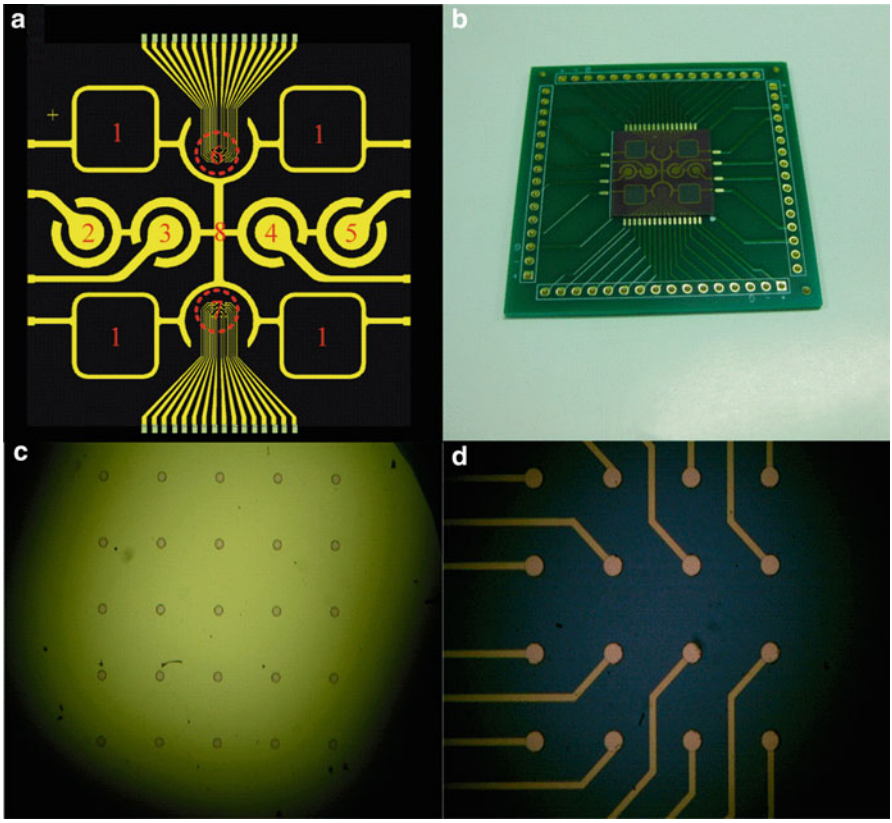

Fig. 8.7 The structure of the hybrid sensor (Reproduced with permission from [11]. Copyright 2013 Elsevier B.V.)

8.3.2 Characterization of MEA

Gold MEA was characterized primarily by cyclic voltammetry to assure electrochemical behavior in SV analysis. Activation procedure was conducted in 0.5 M H_2SO_4 with cyclic voltammetry and the sweep rate was 0.1 V/s. No significant difference was observed in different MEAs and typical cyclic voltammogram was obtained after about 20 times sweep and is shown in Fig. 8.9. Three repetitive cyclic voltammograms present good stability, and well-defined redox reaction of Au-MEA is observed in which oxidation potential (A) and reduction potential (B) are around 1.3 V and 1.0 V.

Subsequent to the activation and cleaning, cyclic voltammetry with different sweep rates (SR) was deployed in 2 mM $K_3[Fe(CN)_6]$ using 0.1 M KCl as the supporting electrolyte. Comparison experiments were conducted between MEAs 2–3 and MEAs 4–5, indicating no significant difference except for the amplitude of

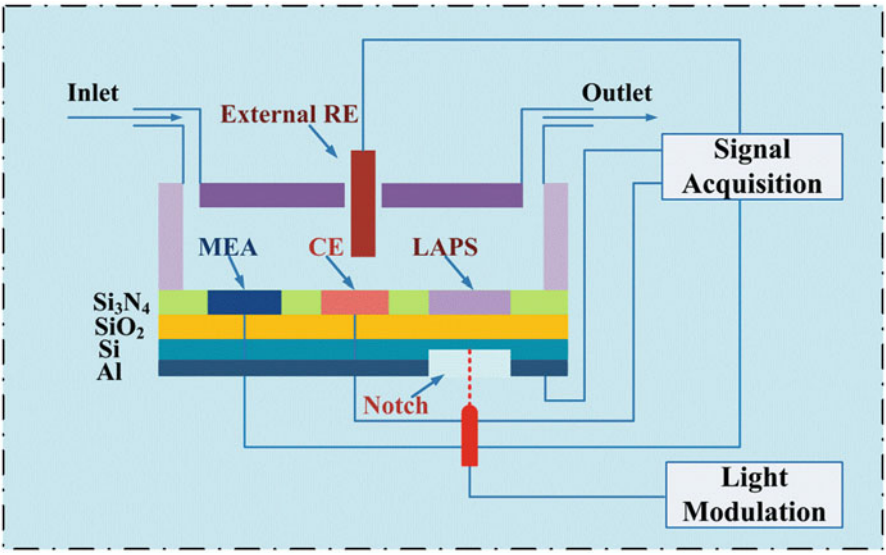

Fig. 8.8 The scheme of the hybrid sensor. *MEA*, *LAPS*, and counter electrode (*CE*) are integrated on the sensor, and signals are acquired through corresponding bonding pads by signal acquisition module (Reproduced with permission from [11]. Copyright 2013 Elsevier B.V.)

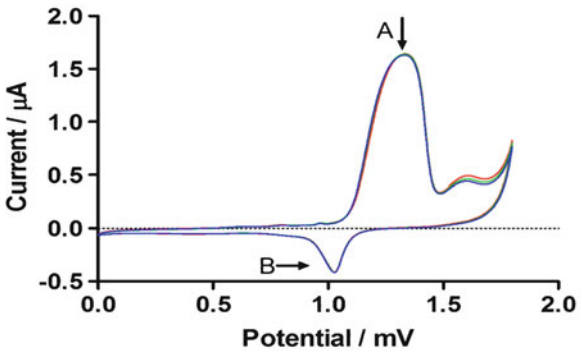

Fig. 8.9 Different MEAs' cyclic voltammograms (Reproduced with permission from [11]. Copyright 2013 Elsevier B.V.)

steady-state current. The difference is attributed to the different numbers of microelectrodes in the array. Therefore, for simplicity, electrochemical behavior of MEA 2 and 3 in Fig. 8.7a was mainly discussed. The cyclic voltammograms of MEA 2 are shown in Fig. 8.10a. Under the condition of low sweep rates, sigmoidal voltammograms were recorded due to the microsize electrode dimensions, and no diffusion overlap occurred in hemispheric diffusion, which is in contrast to macroelectrodes. With the increase of sweep rate, legible peak-shaped voltammogram (SR 0.1 V/s) arose which is in consistent with findings by A. Berduque and coworkers [12]. This is attributed to the decrease of diffusion layer as the increase of sweep rate and monodimensional diffusion became

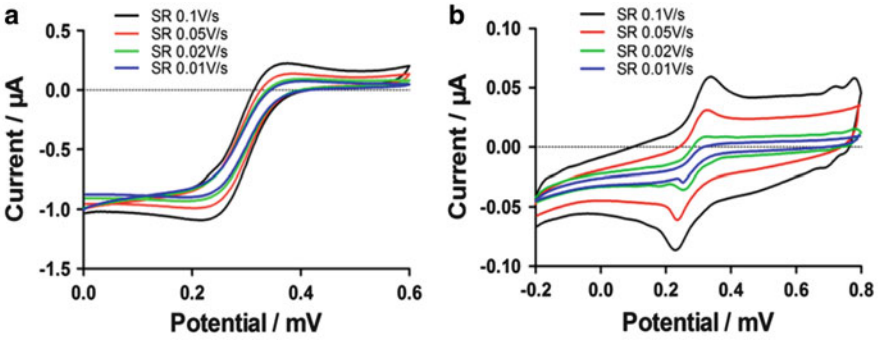

Fig. 8.10 (**a**) The cyclic voltammograms of MEA 2. (**b**) Peak-shaped voltammograms in MEA 3 [11]

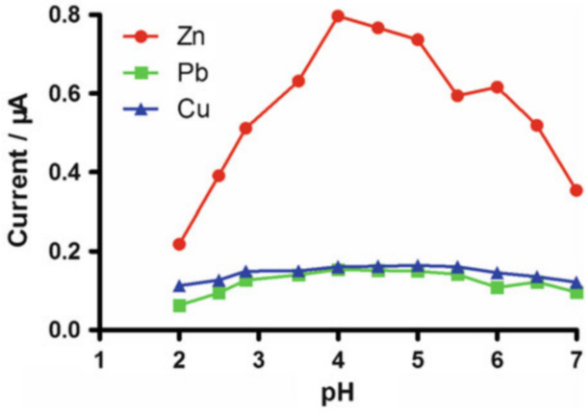

Fig. 8.11 Plots of peak current versus pH (Reproduced with permission from [11]. Copyright 2013 Elsevier B.V.)

predominant similar to macroelectrodes. Peak-shaped voltammograms in MEA 3 with different sweep rates were observed (shown in Fig. 8.10b). This is due to the overlap of diffusion layer with insufficient interelectrode spacing even in high sweep rate. MEA 3 presented a monodimensional diffusion predominantly in analysis of cyclic voltammetry. In summary, characterizations of MEA are affected by the ratio of interelectrode spacing to the size of microelectrode to a great extent. Concerning time costs and maintaining characterizations of microelectrode, MEA 2 was used in further analysis of stripping voltammetry, and the sweep rate was set to 0.05 V/s.

Considering the significant influence of pH variation to the stripping of heavy metal, the impact of different pH on stripping current of heavy metals was discussed to optimize the working condition and utilized for further calibration. Plots of peak current versus pH are shown in Fig. 8.11. As clearly evident, the highest peak current was achieved in the pH range of 4–5, indicating the optimum performance of Au-MEA under solutions with different acidity. When pH was 2, the stripping

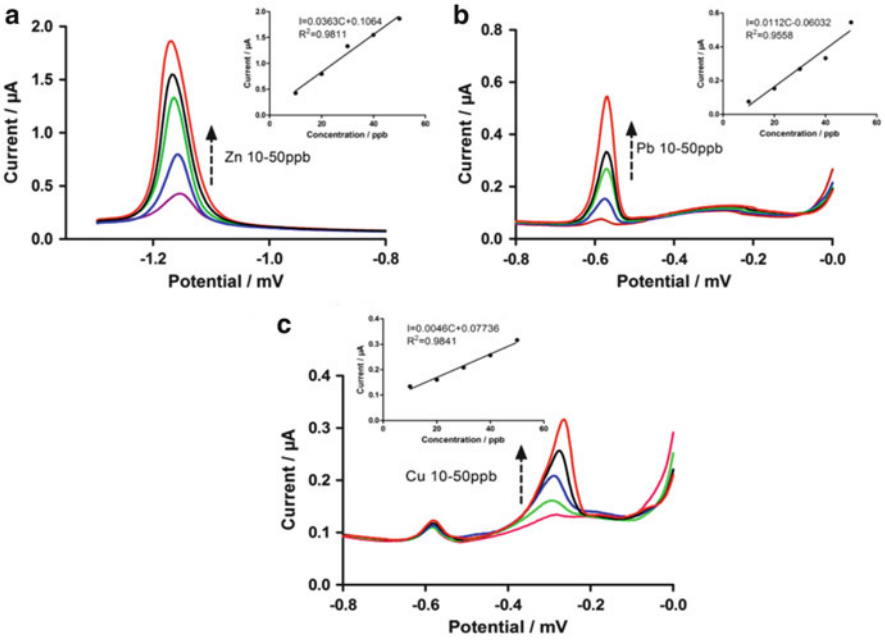

Fig. 8.12 Standard calibration curves of zinc, lead, and copper in 0.5 M KCl with pH 4 acetate buffer (Reproduced with permission from [11]. Copyright 2013 Elsevier B.V.)

peak currents of Zn, Pb, and Cu were relatively low due to the effect of hydrogen reduction. Notably, the peak current of Zn suffered from severe interference attributed to its negative oxidation potential, which approached the reduction potential of hydrogen. The process of hydrogen reduction was dominant on the sensing surface of Au-MEA compared to the oxidation of zinc, thus suppressing the oxidation. The peak current of heavy metal decreased in the pH range of 5–7 and the plausible explanation is the prevailing effect of hydrolysis of heavy metals. Allowing for the stripping currents of Zn, Pb, and Cu with the varying of pH, a pH 4 acetate buffer was applied for further electrochemical analysis.

The standard calibration curves of zinc, lead, and copper were obtained in 0.5 M KCl with pH 4 acetate buffer shown in Fig. 8.12. The deposition potential was −1.35 V and the deposition time was 120 s. The characteristic stripping potentials of zinc, lead, and copper are around −1.1, −0.56, and −0.28 V, respectively. With linear regression, calibration equations for heavy metals were achieved in Fig. 8.12 (inset). The correlation coefficient of zinc is 0.9811 and the sensitivity is 36.3 nA/ppb which is satisfactory for quantitative analysis. The correlation coefficients of lead and copper are 0.9558 and 0.9841, presenting a good linear relationship in the scope of selected concentrations. The sensitivity of lead and copper is 11.2 nA/ppb and 4.6 nA/ppb. The calibration equations acquired by standard curve method (SCM) can be used for quantitative detection of samples and further comparison between different calibration methods.

8.3.3 *Characterization of LAPS*

LAPS on the hybrid sensor was microfabricated for pH detection. The light frequency and light intensity of illuminating light were optimized concerning their vital impacts on the induced photocurrent. The light frequency of 4000 Hz was adopted with best performance and the light intensity was set under the voltage of 1.4 V. In the pH range of 3–8, plots of the photocurrent versus potential were acquired for the calibration of standard curve shown in Fig. 8.13a after normalization. Well-defined drift was observed in the linear working region under solutions with different acidity, suggesting good sensitivity for pH detection. The saturation region and cut-off region were in good coincidence, facilitating the identification of the sensitive point. The sensitive points were located by seeking the inflection point of the I–V curve, and the corresponding potential was recognized as the characteristic value under different pH. The calibration plot of the potential versus pH is shown in Fig. 8.13b. The correlation coefficient between the potential and pH is 0.9986, demonstrating a good linear correlation for pH detection. The sensitivity of LAPS for pH is 52.1 mV/pH, which is in accordance with the Nernst equation for monovalent ion. LAPS presents good sensitivity and performance for pH detection and the typical standard curve is acquired for pH analysis in the samples. To validate the consistency of LAPS, the four sensing areas were all tested for pH detection, and the sensitivity are 50.9 mV/pH, 53.7 mV/pH, and 49.2 mV/pH, respectively. The maximum relative deviation of the sensitivity is less than 5 %, indicating good consistency for pH detection.

The stability and reproducibility of LAPS were evaluated in view of the requirements for practical application. Five repetitive tests were conducted in a sample (pH 7) to validate the behavior of the sensor and the plot is shown in Fig. 8.14a. I–V curves are overlapped in the working region, and slight fluctuations are observed in the saturation region, which is possibly due to the variation of the total ion concentration after each adjustment of pH. The characteristic potential is extracted of which the relative standard deviation (RSD) is 1.45 % in Fig. 8.12 (inset) and good repeatability of plots is presented overall. Subsequently, long-term stability of

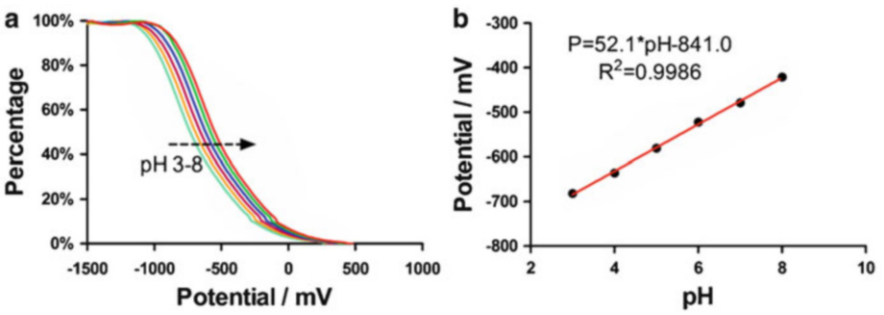

Fig. 8.13 (**a**) The plots of the photocurrent versus potential. (**b**) The calibration plot of potential versus pH [11] (Reproduced with permission from [11]. Copyright 2013 Elsevier B.V.)

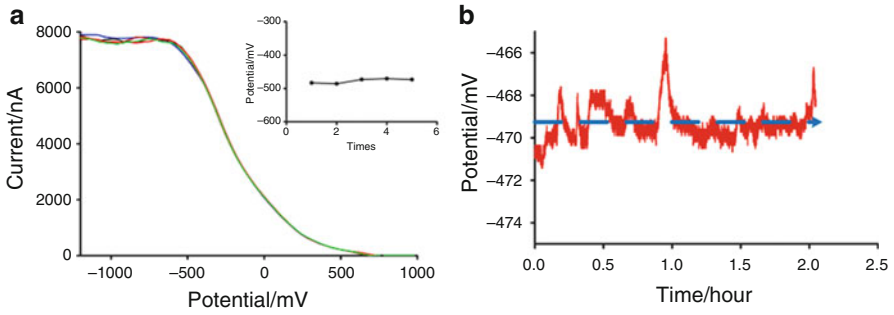

Fig. 8.14 (**a**) The plot of five repetitive tests. (**b**) The deviation of potential versus time (Reproduced with permission from [11]. Copyright 2013 Elsevier B.V.)

LAPS was investigated in a period of 2 h shown in Fig. 8.14b. The deviation of potential in a continuous detection of 2 h is less than 4 mV, while single detection is accomplished in merely 5 min that satisfies practical measurement. LAPS demonstrates good stability and reproducibility for pH detection.

8.4 Application in the Environment and Food Analysis

8.4.1 Heavy-Metal Detection

Electrochemical measurements have shown numerous advantages for trace heavy-metal detection, including rapid analysis, good selectivity, and sensitivity. Therefore, some works related to the electrochemical analysis of ion sensing are discussed in this section [5].

8.4.1.1 Chemically and Biochemically Modified Electrodes

Modified electrodes for electroanalytical determination of heavy metals using stripping voltammetry are commonly employed and present many advantages over the nonmodified electrodes, such as the enhancement of the sensibility and selectivity of the technique. A wide range of modifications have been reported in the literature with the aim of electrochemical detection of heavy metals, ranging from synthetic metal ionophores to biological receptors such as DNA or proteins.

α-Cyclodextrin or *β-cyclodextrin*-modified carbon paste electrodes have been used to determine Pb^{2+} by means of anodic stripping voltammetry [13, 14]. Both modified electrodes display good resolution of the lead oxidation peak. The analysis of the results indicates that the carbon paste electrodes modified with β-cyclodextrin exhibit a better analytical response than the ones modified with *α*-cyclodextrin. Detection limits of 6.30×10^{-7} M and 7.14×10^{-7} M of Pb^{2+},

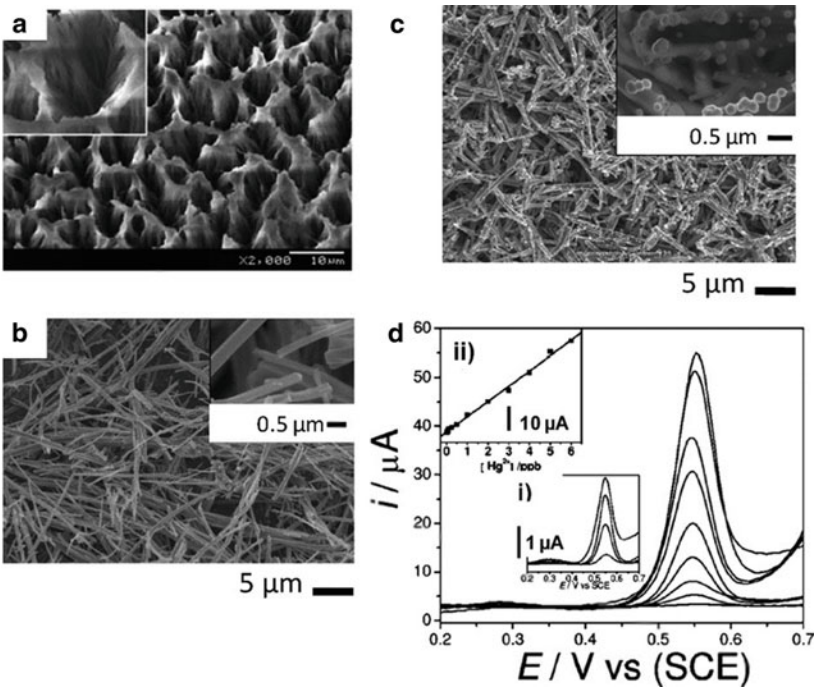

Fig. 8.15 Typical SEM images: (**a**) the bunch-like Bi composed of Bi nanowires, (**b**) the as-synthesized 3,30,5,50-tetramethylbenzidine (*TMB*)-based nanofibers (*NFs*), (**c**) Au-PtNPs/NF inorganic-organic hybrid nanocomposite on a glassy carbon electrode (*GCE*), (**d**) stripping voltammograms of increasing mercury concentrations (Reproduced with permission from [5]. Copyright 2011 American Chemical Society)

respectively, are obtained. The principal factors involved in guesthost complex formation are covalent bonds formed between metal ions and deprotonated $^{-}$O-groups of cyclodextrins.

Although the modified carbon paste electrodes are still being used for sensing purposes, due to their mode of preparation, these devices usually lack reproducibility between batches, and their use is time consuming. While this is not a big problem for in-lab research, it would be a considerable burden in mass production systems.

Because of their exceptional selectivity and sensibility, biomodified electrodes involving DNA, proteins, and antibodies have emerged as a new type of electrochemical sensing strategy for heavy-metal ions. Sensors based on proteins with distinct binding sites for heavy-metal ions are being developed and characterized. A capacitive signal transducer is used to measure the conformational change following heavy-metal binding (Fig. 8.15b). The proteins can be immobilized in different ways on a self-assembled thiol layer on a gold electrode placed as the working electrode in a potentiostatic arrangement in a flow analysis system. Metal ions can be detected down to femtomolar concentration using the biosensor described by

Bontidean et al. [15]. Figure 8.15a shows a developed electrochemical sensor based on cooperative coordination with Hg^{2+} by a pair of short poly-T oligonucleotides that induce conformational switching of the ferrocene-tagged probes from a single-strand to a duplex-like structure, modulating the electron-transfer efficiency [16]. This strategy exploits the cooperation of proximate poly-T oligonucleotides in coordination with Hg^{2+}. Ferrocene (Fc)-tagged poly-T oligonucleotides are immobilized on the electrode surface via self-assembly of the terminal thiol moiety. In the presence of Hg^{2+}, a pair of poly-T oligonucleotides can cooperatively coordinate with Hg^{2+}, which triggers a conformational reorganization of the poly-T oligonucleotides from flexible single strands to relatively rigid duplex-like complexes, thus drawing the Fc tags away from the electrode with a substantial decrease of the redox current. Figure 8.15b1 shows typical differential pulse voltammetry (DPV) curves of the sensor in response to Hg^{2+} ions of varying concentrations, while Fig. 8.15b2 is a plot of DPV peak currents versus Hg^{2+} concentrations. A similar design was proposed for Pb^{2+} detection using methylene blue as electrochemical label [17].

Other approaches related with biochemically modified electrodes involve enzyme-based biosensors, such as oxidase, dehydrogenase, and urease, which detect metal ions by relying on their inhibition of enzymatic reactions [18–20]. The enzyme glucose oxidase has been recently used by Willner et al. (Fig. 8.15c). The system is based on the use of a DNA scaffold for the amplified detection of Hg^{2+} using an electrically contacted relay/enzyme structure as a transducing element [21]. The detection limit for Hg^{2+} corresponds to 100 ± 10 pM. This great sensitivity originates from the amplification path provided by the biocatalytic system. Although the system has high sensitivity, working with enzymes requires narrow operation parameters (e.g., of pH, temperature, ionic strength) and long incubation times. In this context, the application of the enzyme-based system in real samples might be difficult or even impossible if the sample is under extreme conditions. Point-of-care devices are being developed nowadays to provide low-cost analytical systems useful for environmental monitoring of heavy metals. In this context, paper-based systems are highly novel and important [22, 23].

8.4.1.2 Metal Nanoparticle-Modified Electrodes

MNP-modified electrodes may serve as random arrays of microelectrodes. They show distinct advantages over the conventional macroelectrodes, such as increased mass transport, decreased influence of the solution resistance, low detection limit, and better signal-to-noise ratio.

Bismuth and antimony nanoparticles have been proven to be highly sensitive and reliable for trace analysis of heavy metals in conjunction with anodic stripping voltammetry. The attractive and unique behavior of bismuth and antimony nanomodified electrodes is attributed to the formation of multicomponents alloys, as well as the enhanced sensibility coming from the combination of the great

properties of the nanostructured material [24–27]. A new self-organized morphology of Bi (called bunch-like bismuth, see Fig. 8.15a) grown in a bare electrode has been recently described by Zhang et al. and exhibits a good performance for detection of heavy-metal ions [28].

In a parallel way, AuNPs-based electrodes have been proven to be a promising approach for heavy-metal detection [29–31]. Recently, bimetallic NPs have been extensively investigated due to their extraordinary properties, such as good conductivity, and better catalytic activities than their monometallic counterparts. Gong et al. have just reported the use of a bimetallic Au-PtNPs inorganic-organic hybrid nanocomposite-modified glassy carbon electrode for Hg^{2+} ion determination [32]. Bimetallic Au-PtNPs are homogenously distributed in the interlaced nanofiber (NF) matrix (see Fig. 8.15b, c), building a 3D porous network. Such 3D porous nanostructured composite film greatly facilitates electron-transfer processes and the sensing behavior for Hg^{2+} detection, leading to a remarkably improved sensitivity and selectivity. The calibration plot is linear up to 10 ppb, and the detection limit of 0.008 ppb (8 ppt) is obtained with the calculation based on a signal-to-noise ratio equal to 3 (see Fig. 8.15d).

In the same field, Domínguez et al. reported a novel method for the anodic stripping voltammetry determination of Sb^{3+} using AgNPs-modified screen-printed electrodes [33]. The detection limit for Sb^{3+} using the silver and gold modified electrode was 6.79×10^{-10} M for an accumulation time of 200 s.

8.4.1.3 Nanomaterials Combined with Synthetic Receptor-Modified Electrodes

The use of nanomaterials combined with the specific complexing ability of the receptors results in an improved electrochemical sensing platform toward heavy metals with high sensitivity and excellent selectivity for stripping analysis. Pan et al. reported a nanosized hydroxyapatite/ionophore-modified glassy carbon electrode for the determination of lead [34]. The nanostructurated material provides a unique three-dimensional network structure and particular multiadsorbing sites, while the specific complexing ability of the ionophore for lead enhances the sensibility and selectivity of the electrochemical platform for this metal [35]. The electrode has a linear range of response from 5.0 nM to 0.8 μM with a 10 min accumulation time at open-circuit potential. The sensitivity and detection limit of the proposed sensor are 13 μA/μM and 1.0 nM, respectively. Interferences from other heavy-metal ions such as Cd^{2+}, Cu^{2+}, and Hg^{2+} ions associated with lead analysis can be effectively diminished.

A similar work presented by Huang et al. for trace detection of mercury ions combining the use of 2-mercaptobenzothiazole adapters in a SiO_2 3D gold micro/nano pore array has been recently reported showing an excellent linear range (0.05–10 nM) and a good repeatability (relative standard deviation of 2.10 %) [36].

8.4.1.4 Nanobiomodified Electrodes

Electrochemical biosensors based on modifications with DNA and nanomaterials have received increasing attention, mainly for mercury detection [37, 38]. During the past decade, oligonucleotide-functionalized gold nanoparticles have been employed as amplifying tags for novel biosensing protocols due to their unique properties. Recently, Kong et al. have reported a highly selective electrochemical biosensor based on the strong and specific interaction of Hg^{2+} ions by two DNA thymine bases and the use of AuNP-functionalized reporter DNA to achieve signal amplification (see Fig. 8.16a) [39]. The electrochemical mercury biosensor is composed of three elements: a 50-thiol-modified oligonucleotide containing six T-bases for Hg^{2+} binding as a capture probe (DNA 1), an appropriate oligonucleotide linker (DNA 2) with the 30-terminal partially complementary with the capture probe sequence except six T-T mismatches, and finally a DNA 3 functionalized with AuNPs, which could specifically hybridize with the partial linker sequence close to the 50-terminal. When the sensing platform is incubated with solutions containing mercury and the DNA linker, the capture probe can hybridize with the linker via specific T-Hg-T interaction, and the AuNP-functionalized reporter DNA subsequently hybridizes with the linker. In the absence of mercury, the linker does not hybridize with the capture probe, because the melting temperature is lower than

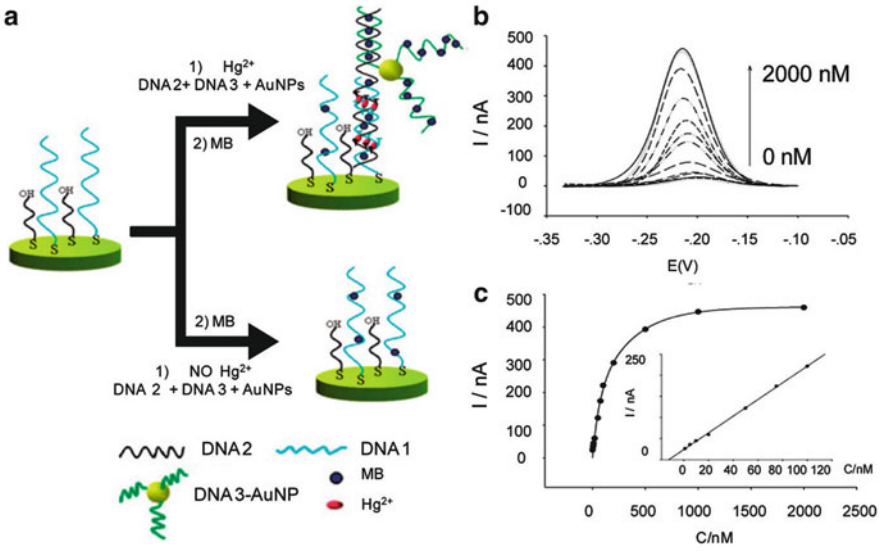

Fig. 8.16 (**a**) A description of the electrochemical Hg^{2+} sensing strategy based on the signal amplification of AuNP-functionalized reporter DNA. (**b**) DPV responses of the sensor after the addition of different concentrations of Hg^{2+} ions. (**c**) Calibration curves of peak current as a function of Hg^{2+} concentration. *Inset*: the linearity of the relative peak current with respect to the Hg^{2+} concentration over the concentration range 1–100 nM (Reproduced with permission from [5]. Copyright 2011 American Chemical Society)

the incubating temperature due to the T-T mismatches. Figure 8.16b shows DPV responses of the sensor after the addition of different concentrations of Hg^{2+} ions (0, 0.5, 1, 5, 10, 20, 50, 75, 100, 200, 500, 1000, and 2000 nM). Moreover, Fig. 8.16c shows the calibration curves of peak current as a function of Hg^{2+} concentration and the linearity of the relative peak current with respect to the Hg^{2+} concentration over the concentration range 1–100 nM. The described electrochemical sensor can achieve a detection limit of 0.5 nM, which makes the detector favorable for Hg^{2+} ion assays in practical samples, such as tap or river water with very low Hg^{2+} concentrations. Even though the system presents low detection limits, issues related with the reusability (by immersing the electrode into 1 M NaOH at 50 C) would represent a drawback for long-term and in-field applications.

8.4.2 Mycotoxin Determination

8.4.2.1 Biosensors as Diagnostic Tools

A biosensor is defined as a bioanalytical device incorporating a molecular recognition element associated or integrated with a physicochemical transducer [40]. To date there are five types of transducers used in biosensor devices, and these include electrochemical, optical, mass-sensitive, calorimetric, and magnetic transducers. The official IUPAC definition states "A biosensor is a self-contained integrated device, which is capable of providing specific quantitative or semiquantitative analytical information using a biological recognition element (biochemical receptor) which is retained in direct spatial contact with a transduction element" [41]. Figure 8.17 shows the concept of constructing a biosensor device where a biorecognition material is selected and then immobilized on the chosen sensor platform surface. The assay is then developed and optimized, and this is then combined with the instrument which will produce the digital signal. The use of these devices allows the capability of analyzing food and feed samples on-site such as on the farm or at the food factory [42]. That is because biosensors have the advantages over traditional methods of being, simple, rapid, cost-effective, and portable devices that are sensitive and specific for the target analyte, e.g., the mycotoxin. These devices can also be designed to be disposable for single use and reusable for several analyses or for continuous monitoring. A range of biosensors have now been developed and reported in the literature for mycotoxin analysis, some of which have the capability of multi-array mycotoxin diagnosis (multiplexing capabilities). The sample preparation can usually be incorporated as part of the sensor procedure system. Some of the extraction and cleanup procedures may be similar to the procedures used for HPLC or GC analysis especially if the samples are of solid food nature. Some sensors have been developed to be applied directly for liquid samples without the need for extraction of the sample. To date sensors can be designed to handle the sample through the inclusion of a microfluidic

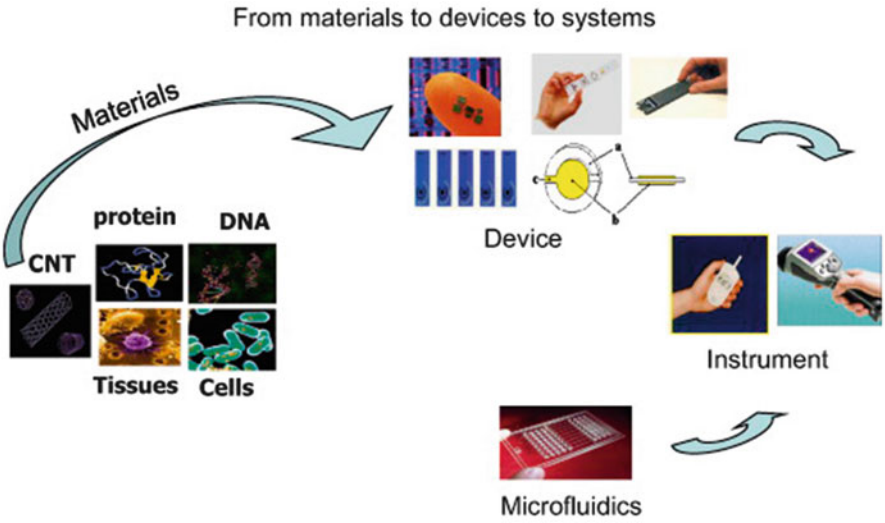

Fig. 8.17 Biosensor construction: a biorecognition material is selected and immobilized on the chosen sensor platform surface, then the assay is developed and optimized and this is then combined with the instrument which will produce the digital signal (Reproduced with permission from [43]. Copyright 2009 Elsevier Ltd.)

system or membrane separation system as part of their design for extracted food sample handling.

8.4.2.2 Micro/Nano electrode Arrays

Nanotechnology has the potential to improve food quality and safety significantly through the use of advanced micro- and nanosensors and tracking systems. Nanotechnology is research at the interface between chemistry, biology, material science, physics, and engineering where ultraprecision engineering can be combined with nanostructured materials and molecular manipulation to produce novel devices. The National Nanotechnology Initiative (NNI) defines nanotechnology as "Research and technology development at the atomic, molecular or macromolecular scale leading to the controlled creation and use of structures, devices and systems with a length scale of 1–100 nanometers (nM)" [44]. Interest in nanotechnology relies on the new properties that materials exhibit when reduced to the nanometer scale compared to the bulk materials. Lab-on-a-chip devices are examples of micro/nano technology systems approaches which can be used for the analysis of food contaminants such as mycotoxins for on-site analysis. These devices can be cost-effective and highly beneficial for the food industry in ensuring high safety and quality of the food and also for risk assessment and management. The use of nanomaterials and structures such as semiconductors and conducting polymer nanowires and nanoparticles (carbon nanotubes, silica nanoparticles,

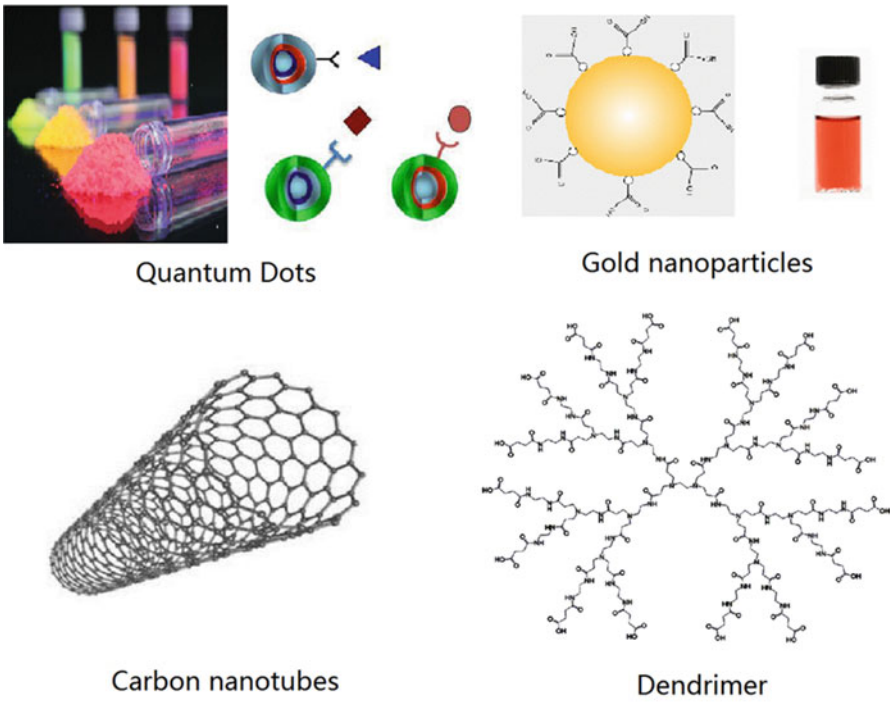

Fig. 8.18 Examples of nanoparticles used in sensor developments: they are quantum dots, carbon nanotubes, gold nanoparticles, and dendrimer

dendrimers, noble metal nanoparticles, gold nanoshells, superparamagnetic nanoparticles, quantum dots, polymeric nanoparticles) for biosensor applications is expanding rapidly. Figure 8.18 shows examples of some nanoparticles used for sensor applications. To date many comprehensive review articles have been published in this area [45–48].

The development of micro/nano sensor devices for toxins analysis is increasing due to their extremely attractive characteristics for this application. In principle these devices are miniature transducers fabricated using conventional thin and thick film technology. Their novel electron transport properties make them highly sensitive for low-level detection [49, 50]. The multiplex analysis capability is also very attractive for multi-biomarker analysis. Micro/nano electrodes can be classified as small electrodes in which at least one dimension is in the μm or nm range, respectively. These can also be fabricated using different materials such as platinum, gold, iridium, and carbon on silicon wafers. Microelectrode arrays (MEA) have been fabricated to produce miniaturized electrochemical sensors [12, 51]. Different shapes and sizes of these electrodes have been fabricated using standard deposition, etching, lithography, and photolithography techniques, including micro-disk electrodes [52], microband electrodes [53], interdigitated electrodes, and three-dimensional MEA [54]. The devices can be based on macro-type of

transducers such as receptor spots on glass slide or can be easily fabricated using screen-printing technology with multi-working electrode array. In order to develop practical devices for commercial developments, problems of binding between heterogeneous antigens and antibodies used in the sensor assays and also the high background signals need to be eliminated and controlled. Multi-toxin detection (e.g. mycotoxins) in foods can be conducted using single micro/nano electrode array chip with high sensitivity and rapid analysis time. The use of micro/nano arrays for analysis applications in foods can produce highly sensitive sensors.

Multi-mycotoxin detection has also been reported in the literature using different sensor platforms combined with multi-ELISA assays. Therefore, multi-toxins can be detected on a single microelectrode array chip with multi-array working electrode, where different antibody is immobilized to detect a specific mycotoxin. Micro/nano electrode arrays have unique properties which include small capacitive charging current and faster diffusion of electro-active species which will result in an improved response time and greater sensitivity [12]. The use of lab-on-a-chip is expanding in all areas of analysis due to the advantages of using small samples to analyze several markers/toxins, i.e., offer high-throughput analysis [55]. These types of devices will be attractive for mycotoxin analysis since several toxins may exist in the same food or feed sample. Examples are the electrochemical assay developed by Piermarini et al. [56], using a 96 well screen-printed microplate to detect aflatoxin B1 in corn samples. Detection was carried out using alkaline phosphatase as the label enzyme with the array used to detect the toxins in several samples simultaneously. Other examples of multi-mycotoxin analysis sensors include those reported by Ngundi et al. [57, 58], using a fluorescence-labeled antibody with a sensor arrays to detect ochratoxin A and deoxynivalenol. Also Gaag et al. [59] developed an SPR biosensor array to monitor aflatoxin B1 and deoxynivalenol. However, no real samples were analyzed using this sensor. Ligler et al. [60] reported on the use of biosensor consisting of a patterned array of capture antibody immobilized on planar waveguide. A fluorescent assay is then performed and the spots are captured using a CCD camera. Several authors reported the use of competitive immunofluorescent assays on a biosensor array for the simultaneous detection of several mycotoxins such as aflatoxin B1, fumonisin, ochratoxin A, and deoxynivalenol [60, 61]. Recently, Bayer Technology Services GmbH has developed a mycotoxin biochip platform based on planar waveguide technology, which is able to analyze multiple mycotoxins based on fluorescently labeled antibodies and consists of a reader and a lab-on a-chip cartridge.

We have developed an electrochemical microarray with 35 arrays and which was used for the detection of aflatoxin M1 [62] (Fig. 8.19). Each array consisted of 35 microsquare electrodes with 20×20 μm dimensions and edge-to-edge spacing of 200 μm (an electrode width to spacing ratio of 10). These dimensions and spacings were chosen to avoid overlapping diffusion layers between neighboring electrodes in the array. The whole microarray was used to immobilize the antibody for aflatoxin M1 analysis with very sensitive detection limit achieved (8 ng L-1 in milk) using amperometry as the detection system. This has now been also used for aflatoxin B1 and fumonisin detection (unpublished data). The use of microarrays

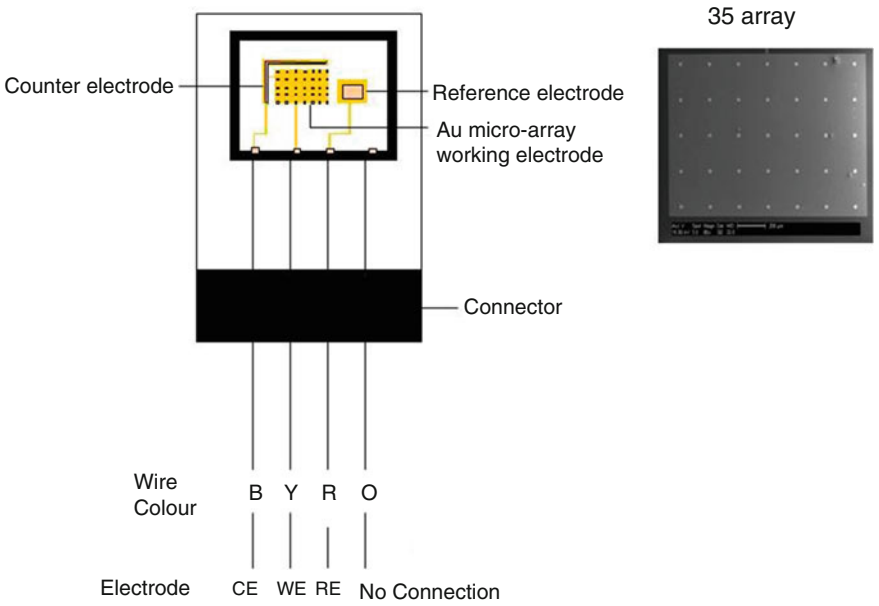

Fig. 8.19 A three-electrode chips with a working electrode area (35 electrodes in the array), a counter electrode, and a reference electrode area (Reproduced with permission from [62]. Copyright 2009 American Chemical Society)

for mycotoxin analysis is still progressing, and as shown above it can produce very highly sensitive sensors for mycotoxin analysis.

8.4.3 Application of the LAPS

The LAPS was first proposed by Hafeman in 1988 as a semiconductor device for biochemical systems [63, 64]. In the following 20 years, LAPS was widely studied in biological analysis and commonly used as an ISFET [65]. Different LAPS systems are designed to obtain better sensitivity, stability, and compatibility for bioassays. The cytosensor microphysiometer for extracellular acidification and the threshold unit for immunoassays have been commercialized by Molecular Devices Corp. (Sunnyvale, CA) [64]. The potentiometric alternating biosensor system has also been commercialized by Technobiochip (Marciana, Livorno, Italy) [66]. These systems have been used widely in various areas, including cellular physiology, toxicology, and pharmacology.

8.4.3.1 Typical LAPS

An LAPS is typically structured as a conventional electrolyte-insulator-semiconductor (EIS) sensor (Fig. 8.20a) [65], and the LAPS surface is chemically deposited with silicon oxynitride as an insulating layer, which can also be silicon oxide and silicon nitride. The insulating layer separates the silicon chip from the solution. The sensor surface forms silamine and silanol groups under hydration. The solution pH can affect the surface potential by changing the proportion of silamine and silanol groups. In the high-pH condition, the LAPS surface has a strong negative charge. In the low-pH condition, the LAPS surface has a weak charge. An electric field is generated in the LAPS when a DC voltage is applied on the sensor chip. A photocurrent is produced by a pulsing infrared light from a light-emitting diode (LED) at the backside of the chip. The photocurrent amplitude depends on the sum of the surface potential and applied potential, and the former depends on the solution pH of the insulating layer [67] (Fig. 8.20b). In the conventional detection mode, a DC voltage is used to keep the LAPS photocurrent constant, and the voltage changes correspond to the pH changes (60 mV/pH unit). Therefore, biological events could induce corresponding fluctuations in the photocurrent output by modifying the electrochemical parameters of the interface.

In the biological application, the LAPS commonly monitors the cellular metabolism, especially energy metabolism. The heterotrophic cells obtain various

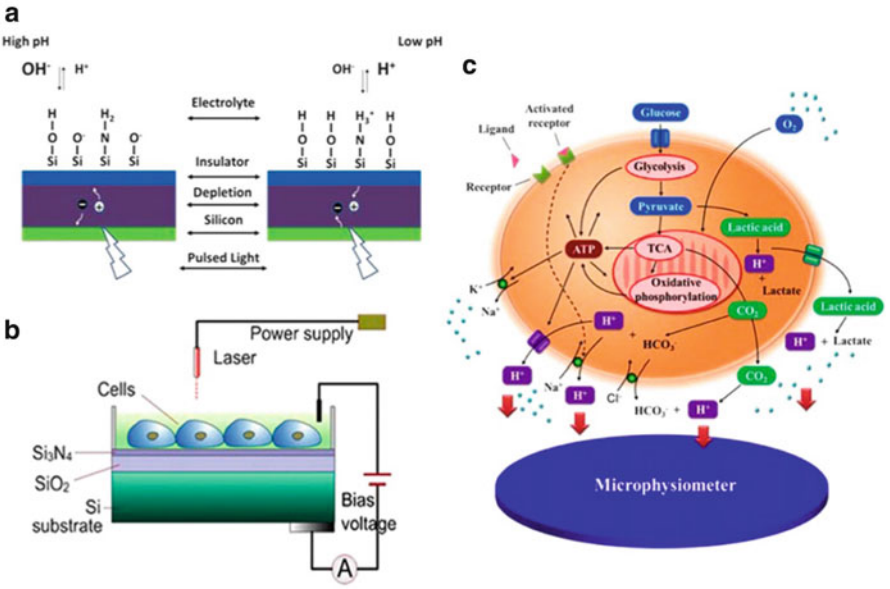

Fig. 8.20 Illustration of a LAPS as a microphysiometer: (**a**, **b**) principle and structure of the LAPS (Reproduced with permission from [65]. Copyright 2000 Elsevier S.A.) (**c**) proton release in cellular metabolism (Reproduced with permission from [67]. Copyright 2011 Elsevier B.V.)

nutrients, produce the energy, and release the wastes for growth. The carbon source (e.g., sugars, amino acids, and fatty acids) mainly produces metabolic energy. The schematic overview of the cellular metabolic process is presented in Fig. 8.20c. In the natural aerobic condition, cells convert glucose into CO_2. In the anaerobic condition, cells convert glucose into lactic acid. The acidic products (e.g., H+, CO_2, and lactic acid) generated by cellular energy metabolism induce a pH drop in the extracellular microenvironment, which can be detected by a microphysiometer.$_{309}$ On the basis of this principle, a large amount of experiments have been carried out to monitor the extracellular acidification rate (ECAR), which is the most significant parameter indicating the state of cellular metabolism. Many biochemical factors, such as receptor-ligand reactions, will affect the ECAR of the cells, and the effects of these factors can be measured via a microphysiometer. Additionally, a microphysiometer can analyze and evaluate pharmaceutical effects on ECAR, such as antitumor drugs for chemotherapy [68, 69].

In constructing cell-based biosensors for extracellular microenvironment monitoring, the LAPS is preferred over the ISFET because of its compatibility with MEMS fabrication, less critical and easier encapsulation, and incorporation into microvolume measuring chambers for bioassays. Also, when cells are cultured on a silicon surface, extracellular action potential coupled to the sensor surface can also generate corresponding spikes in the photocurrent output [70]. Electrophysiological study with the LAPS can overcome the geometric restrictions of MEAs and FETs.

8.4.3.2 Microphysiometers Based on the LAPS

The LAPS is sensitive to pH variation in the electrolyte solution. By encapsulating the LAPS and cells in a microvolume chamber, the microphysiometer is used to indicate the ECAR (Fig. 8.21) [71]. In the microphysiometer, cells are cultured in the microvolume chamber, which is formed by a multiporous polycarbonate membrane and an O-ring spacer. The microvolume chamber is tightly fixed on the LAPS chip, and H+ can diffuse adequately in the small volume, so the ECAR can be directly measured by the LAPS. A modulated infrared LED (light-emitting diode) illuminates the backside of the LAPS, and thus, the LAPS will generate a photocurrent with the same frequency. All of the experimental data are transmitted into a computer by the detection and analysis instrument. The culture medium is injected into the flow chamber by the peristaltic pump, the degasser, and finally the injection valve. The ECAR can be continually measured by refreshing the culture medium cycle.

The basic function of the microphysiometer is to study the metabolic activities responsive to agents. The metabolic activity responses of different cells to many different agents have been successfully monitored [72, 73]. For example, for fibroblast cells, 2-deoxy-D-glucose reduces the acidification rate from −90 to −40 μV/s, which is directly induced by the decrease of lactic acid. Also, fluoride acts as a metabolic inhibitor which binds to the enolase and affects pyruvate formation, which subsequently decreases the ECAR significantly.

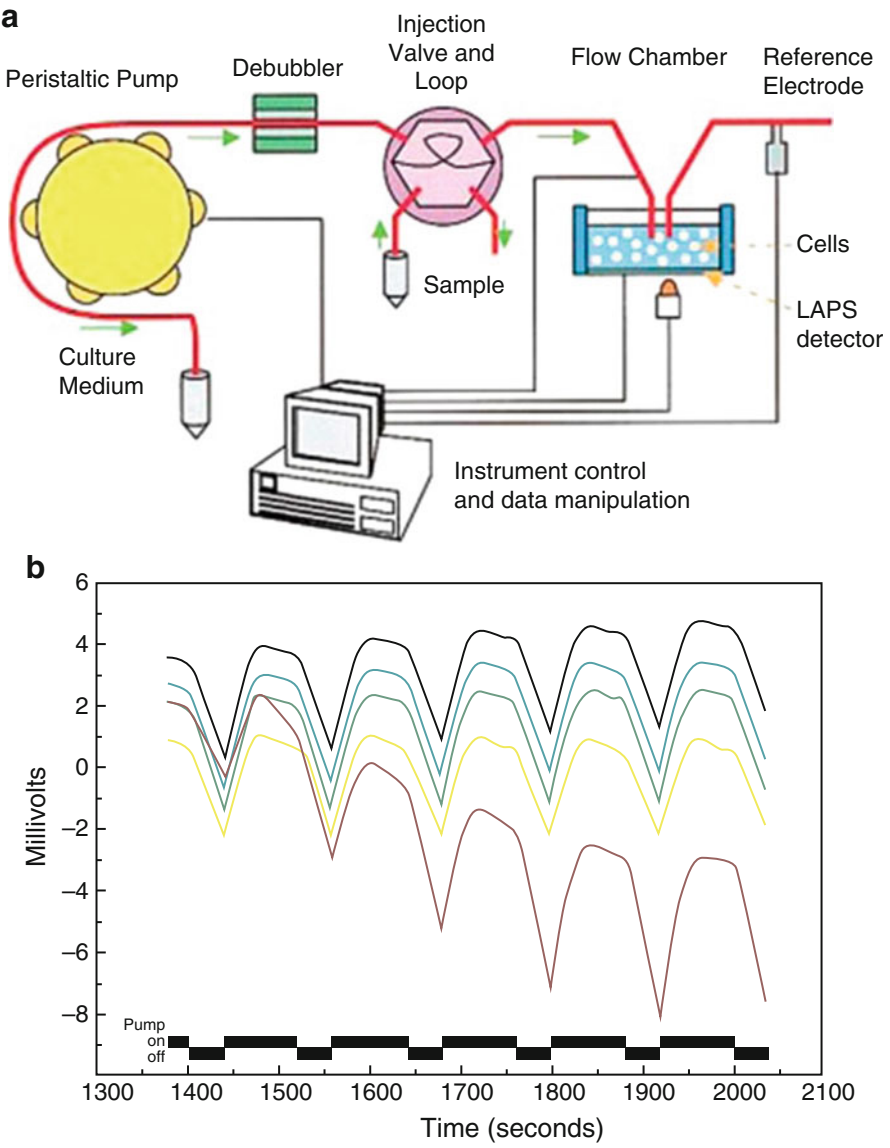

Fig. 8.21 Microphysiometer for extracellular acidification based on the LAPS: (**a**) schematic of the cytosensor microphysiometer, (**b**) ECAR measured by the flow-on/flow-off cycle of the microphysiometer (Reproduced with permission from [71]. Copyright 1999 John Wiley & Sons, Inc.)

Changes in the ECAR typically ranged from 110 to 200 % of the basal ECAR in the receptor activations [74]. Pharmacology assays with microphysiometers can measure the functional consequence of extracellular acidification by drugs binding to molecules. Additionally, microphysiometers can measure the ECAR induced by many receptors (e.g., cAMP and mitogenesis). Cells maintain homeostasis by releasing H+, so the overall cellular metabolism can be reflected by the ECAR. Applications have been proposed in studies including pharmacology-related signaling mechanisms [75], functional characterizations of ligand-receptor binding [76, 77], and identification of specific and functional orphan receptors [78, 79]. Many activations of protein tyrosine kinases have been investigated using the effects of pharmacological factors and receptors, such as epidermal growth factor (EGF) receptor tyrosine kinase [75, 76], epidermal growth factor [80], insulin-like growth factor-1 (IGF-1) [81], ligand-gated ion channels [82], leptin receptor [83], T-cell receptor [84], G-protein-coupled receptors of angiotensin II receptor, type 1 (AT1) receptor [85, 86], and bradykinin receptor B2 [87].

When the signaling pathways are coupled, the receptor activation-induced cellular responses can be studied with the ECAR. For example, dimethyl amiloride (DMA) was used to study Na^+/H^+ exchanger activities in cells growing at different cell densities [88]. Exposing cells at low density (10^4 cells/mL) to dust induced an initial release of acid not involving the exchanger, followed by a sustained DMA-sensitive Na^+/H^+ exchanger activation. In cells near high density (10^6 cells/mL), the Na^+/H^+ exchanger was not activated during exposure, resulting in a modest increase in the ECAR. Exposing cells at high density resulted in a biphasic ECAR pattern, and an initial increase in proton release was followed by an inhibition of the ECAR below baseline. Polar amino acids are important in the proton flux activity of Na^+/H^+ exchangers [89]. A large number of G-protein- and non-G-protein-coupled hormone and neuropeptide receptors which activate the signal transduction mechanisms have been investigated [90]. Signal pathways of gp130 family cytokines (interleukin-6 (IL-6), oncostatin M) and IL-1 were probed by the ECAR of HepG2 cells [91]. Extracellular acidification measurement is a kind of in vitro bioassay, and H+ is used as an indicator of overall cellular metabolism. Initial studies of irritancy testing using human keratinocytes grown on coverslips tested half-log serial dilutions of eight irritants previously characterized as having in vivo ocular irritancy ranging from mild to severe [92]. Ocular and skin irritancy testing materials represent the range of effects commonly encountered in cleaning products [93, 94]. Other cell sources, including hepatic cells and cancer cell lines [91, 95], were treated with various toxins and drugs to evaluate their effects. The microphysiometer is a useful platform to monitor metabolic disturbance by measuring the recovery of the extracellular microenvironment.

Further improvements of the microphysiometer system were proposed for monitoring several parameters in the extracellular microenvironment related to ATP usage and metabolic processes. A multianalyte microphysiometer has been proposed to simultaneously measure the acidification rate, glucose consumption, oxygen uptake, and lactate production in the extracellular environment by modifying the cytosensor microphysiometer system to study the cellular metabolism more

comprehensively [72, 73]. Another attempt to use a multiparameter microphysiometer was made using poly(vinyl chloride)-based ion-sensitive membranes on the LAPS surface for extracellular monitoring of ions such as K^+, Na^+, Ca^{2+}, and Cl− [96, 97]. These multianalyte and multiparameter detections can provide more biological information about cellular responses to achieve better evaluation of drug effects. Especially, if modified with a porous structure, the LAPS could display highly enhanced performance attributed to morphological changes in the sensing units [98].

8.4.3.3 Cell-Semiconductor Hybrid for Electrophysiological Detection

In the above section, the microphysiometer is introduced to monitor metabolism in a cell population. However, it is far from the ability of cell-semiconductor hybrid systems to detect ion channels or potentials of cells. The LAPS surface is totally flat without any special structures, so the cells can easily culture and freely attach to the LAPS. Recently, the LAPS was used to study excitable cells by monitoring extracellular potentials [99, 100]. In principle, the modulated infrared laser is focused by the microscope to illuminate the position of the target cell. The inflow or outflow of cellular ionic currents (e.g., Na^+, K^+, and Ca^{2+}) will induce fluctuation of the LAPS response signals.

The LAPS consists of an EIS structure (Fig. 8.22a, b) [101]. The insulator (SiO_2 layer) is suitable for the attachment of cells without the addition of special structures. Therefore, the ionic current induced by the extracellular potential will couple with the LAPS surface, and the corresponding photocurrent change can be detected by the LAPS. This simple model of the cell-sensor interface is shown in Fig. 8.22c. The LAPS has the light-addressable function, and the laser can scan at arbitrary positions on the LAPS surface. On the basis of the working principle, the extracellular potential of the cell can be detected when the focused laser illuminates the sensitive region of a cell [101]. Thus, a membrane potential change can cause

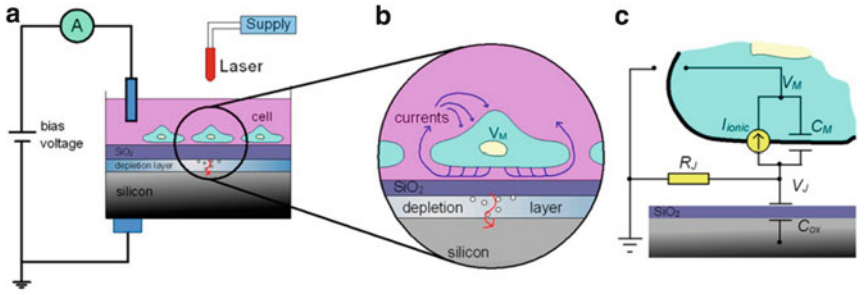

Fig. 8.22 Extracellular potential monitored with the LAPS: (**a**) schematic of the cell-based biosensor and LAPS detection system, (**b**) cell-sensor interface with the EIS structure, (**c**) simplified model of the cell-LAPS biosensor (Reproduced with permission from [101]. Copyright 1999 2006 Elsevier B.V.)

corresponding turbulence in the LAPS output. In recent research, cell-LAPS hybrid biosensors have been proposed as superior instruments for extracellular recording of potential signals [70, 99, 102, 103]. Most recordings were performed with excitable cells, such as ardiomyocytes and neurons.

As discussed in this review, the FET array and MEA are at present the two main types of cell-semiconductor hybrid biosensor systems for extracellular detection. However, the MEA and FET are typically restricted by their surface structure because only a few electrodes are fabricated. Thus, a small effective detection region can be used to monitor the cellular state. Moreover, microelectronic fabrication restricts the distance of the electrodes on the MEA and FET [104], which ranges from 50 to 200 μm [100]. Consequently, the spatial resolution of the sensor is restricted significantly, and it will hamper the development of the biosensors. However, the LAPS is different from the MEA and FET due to its special working mode. The surface potential of the LAPS can be monitored and detected by a scanning focused laser beam. The illuminated site will generate a photocurrent signal which reflects the surface potential. Taking this characteristic into consideration, the spatial resolution will be much improved. Therefore, an arbitrary site on the LAPS can sense the cellular state, so all of the cells cultured on the LAPS can be studied.

The majority of related studies are focused on self-exciting cells such as neurons and cardiomyocytes [105]. Stem cells and tissues are also used as new sources for LAPS biosensors [67, 106, 107]. Liu et al. have cultured the mouse embryoid bodies on the LAPS and induced them to differentiate into cardiomyocytes and neurons in vitro (Fig. 8.23a) [67]. Typical signals of cardiomyocytes recorded are shown in Fig. 8.23b. The spikes can be sorted and analyzed by several parameters shown in Fig. 8.23c. Differences in these parameters can reflect cellular responses to drugs in a way similar to that of MEA- and FET-based biosensors. Electrophysiological responses are monitored using amiodarone, noradrenaline, sparfloxacin, and levofloxacin as cardiotoxic drugs.

An obvious disadvantage of the LAPS is its single-channel output, which makes it difficult to record extracellular potentials of multisite cells simultaneously. The LAPS with submicrometer electrodes has been reported with a light-addressable function [108]. This novel design concept will even benefit MEA systems to solve the problem of lower spatial resolution. Moreover, the functions and performance of the LAPS can be enhanced by modifying specific bioactive units and other materials, such as biological enzymes and ion-selective membranes, to detect many physiological parameters of cells simultaneously.

Alongside parallel detection, another promising field is using the LAPS as a virtual electrode to stimulate excitable cells. The extracellular potential is determined by the membrane potential and ionic current. One group has developed the LAPS biosensor technology by recording the extracellular stimulations of discrete neurons [109]. The complicated spatiotemporal patterns of cell networks can be investigated by scanning the desired sites on the LAPS. Therefore, information at any site will be monitored continually. Compared to the site-restricted MEA, the LAPS can serve as a useful biosensor to carry out the spatiotemporal analysis.

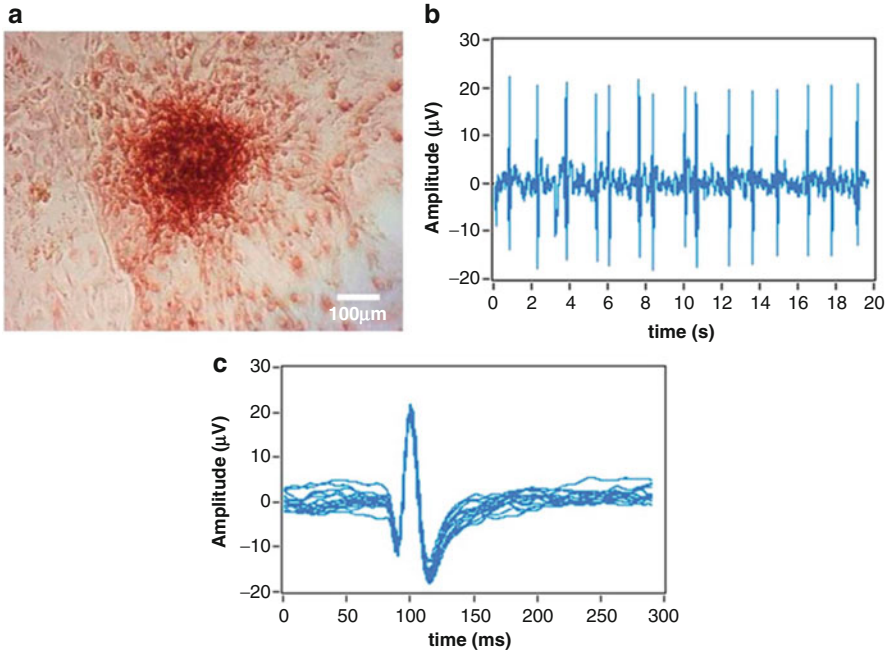

Fig. 8.23 Embryonic stem cells differentiated into cardiomyocytes and extracellular potentials detected by the LAPS: (**a**) mouse embryoid bodies differentiated into cardiomyocytes on the LAPS, (**b**) typical signals recorded, (**c**) automatic spike sorting (Reproduced with permission from [67]. Copyright 2011 Elsevier B.V.)

Additionally, visualized research on cells and tissues may be improved by the technology. The bioelectronics and bioelectrochemical imaging will facilitate the study of cell networks with the development of spatiotemporal pattern studies.

The cell-silicon junction plays a significant role in the combination of neuronal dynamics and electronics. The integration of excitable cells and sensors will be used to exploit a new approach for both eliciting and recording neuronal networks on the same chip simultaneously. The neuronal networks can be formed on the sensors, and the signaling pathway of the neuronal networks can also be modeled and computed in further investigations.

8.5 Summary

The developments in micro/nano electrochemical sensors have large impact on ion sensing research. Significant advances in the fabrications of micro/nano electrochemical sensors are being persistently made. In this chapter, we briefly described the theory of electrochemical sensors for ion sensing, which contain potentiometric sensors, voltammetric sensors, and microelectrode array. A detailed analysis of

these sensors has been carried out on the latest research advancement made in the development of ion sensing-based sensors/biosensors. The characteristics of these sensors are also described in detail.

As more and more nanomaterials were discovered and used, micro/nano electrochemical sensors have become a new detection technology. It has broad application prospect in the field of environment and food analysis. The application of LAPS, heavy-metal detection, and mycotoxin determination has been described in detail in this chapter.

References

1. Goyer RA. Nutrition and metal toxicity. Am J Clin Nutr. 1995;61(3):646S–50.
2. Goyer RA, Clarkson TW. Toxic effects of metals', Casarett & Doull's toxicology. In Klaassen, CD, editor.The basic science of poisons, 5th ed. McGraw-Hill Health Professions Division, New York; 1996. ISBN, 71054766.
3. Goyer RA. Toxic and essential metal interactions. Annu Rev Nutr. 1997;17(1):37–50.
4. Gaetke LM, Chow CK. Copper toxicity, oxidative stress, and antioxidant nutrients. Toxicology. 2003;189(1):147–63.
5. Aragay G, Pons J, Merkoci A. Recent trends in macro-, micro-, and nanomaterial-based tools and strategies for heavy-metal detection. Chem Rev. 2011;111(5):3433–58.
6. Wang P, Liu Q, Wu C, Hsia KJ. Bioinspired smell and taste sensors. In Editor (Ed.)^(Eds.). Book bioinspired smell and taste sensors. Dordrecht: Springer; 2015, edn. pp.
7. Campos I, Pascual L, Soto J, Gil-Sánchez L, Martínez-Máez R. An electronic tongue designed to detect ammonium nitrate in aqueous solutions. Sensors. 2013;13(10):14064–78.
8. Weber SG. Signal-to-noise ratio in microelectrode-array-based electrochemical detectors. Anal Chem. 1989;61(4):295–302.
9. Ramos A, Morgan H, Green NG, Castellanos A. Ac electrokinetics: a review of forces in microelectrode structures. J Phys D Appl Phys. 1998;31(18):2338.
10. Davies TJ, Compton RG. The cyclic and linear sweep voltammetry of regular and random arrays of microdisc electrodes: theory. J Electroanal Chem. 2005;585(1):63–82.
11. Wan H, Ha D, Zhang W, Zhao H, Wang X, Sun Q, Wang P. Design of a novel hybrid sensor with microelectrode array and LAPS for heavy metal determination using multivariate nonlinear calibration. Sens Actuators B. 2014;192:755–61.
12. Berduque A, Lanyon YH, Beni V, Herzog G, Watson YE, Rodgers K, Stam F, Alderman J, Arrigan DW. Voltammetric characterisation of silicon-based microelectrode arrays and their application to mercury-free stripping voltammetry of copper ions. Talanta. 2007;71(3):1022–30.
13. Norkus E. Metal ion complexes with native cyclodextrins. An overview. J Incl Phenom Macrocycl Chem. 2009;65(3–4):237–48.
14. Fragoso A, Ortiz M, Sanromà B, O'Sullivan CK. Multilayered catalytic biosensor self-assembled on cyclodextrin-modified surfaces. J Incl Phenom Macrocycl Chem. 2011;69(3–4):355–60.
15. Bontidean I, Berggren C, Johansson G, Csöregi E, Mattiasson B, Lloyd JR, Jakeman KJ, Brown NL. Detection of heavy metal ions at femtomolar levels using protein-based biosensors. Anal Chem. 1998;70(19):4162–9.
16. Liu S-J, Nie H-G, Jiang J-H, Shen G-L, Yu R-Q. Electrochemical sensor for mercury (II) based on conformational switch mediated by interstrand cooperative coordination. Anal Chem. 2009;81(14):5724–30.

17. Xiao Y, Rowe AA, Plaxco KW. Electrochemical detection of parts-per-billion lead via an electrode-bound DNAzyme assembly. J Am Chem Soc. 2007;129(2):262–3.
18. Zhylyak G, Dzyadevich S, Korpan Y, Soldatkin A, El'Skaya A. Application of urease conductometric biosensor for heavy-metal ion determination. Sens Actuators B. 1995;24 (1):145–8.
19. Rodriguez BB, Bolbot JA, Tothill IE. Development of urease and glutamic dehydrogenase amperometric assay for heavy metals screening in polluted samples. Biosens Bioelectron. 2004;19(10):1157–67.
20. Fennouh S, Casimiri V, Geloso-Meyer A, Burstein C. Kinetic study of heavy metal salt effects on the activity of L-lactate dehydrogenase in solution or immobilized on an oxygen electrode. Biosens Bioelectron. 1998;13(7):903–9.
21. Mor-Piperberg G, Tel-Vered R, Elbaz J, Willner I. Nanoengineered electrically contacted enzymes on DNA scaffolds: functional assemblies for the selective analysis of Hg^{2+} ions. J Am Chem Soc. 2010;132(20):6878–9.
22. Nie Z, Deiss F, Liu X, Akbulut O, Whitesides GM. Integration of paper-based microfluidic devices with commercial electrochemical readers. Lab Chip. 2010;10(22):3163–9.
23. Tan SN, Ge L, Wang W. Paper disk on screen printed electrode for one-step sensing with an internal standard. Anal Chem. 2010;82(21):8844–7.
24. Rico MÁG, Olivares-Marín M, Gil EP. Modification of carbon screen-printed electrodes by adsorption of chemically synthesized Bi nanoparticles for the voltammetric stripping detection of Zn (II), Cd (II) and Pb (II). Talanta. 2009;80(2):631–5.
25. Lee G-J, Lee HM, Uhm YR, Lee MK, Rhee C-K. Square-wave voltammetric determination of thallium using surface modified thick-film graphite electrode with Bi nanopowder. Electrochem Commun. 2008;10(12):1920–3.
26. Stozhko NY, Malakhova NA, Fyodorov MV, Brainina KZ. Modified carbon-containing electrodes in stripping voltammetry of metals. J Solid State Electrochem. 2008;12 (10):1185–204.
27. Toghill KE, Xiao L, Wildgoose GG, Compton RG. Electroanalytical determination of cadmium (II) and lead (II) using an antimony nanoparticle modified boron-doped diamond electrode. Electroanalysis. 2009;21(10):1113–8.
28. Zhang Z, Yu K, Bai D, Zhu Z. Synthesis and electrochemical sensing toward heavy metals of bunch-like bismuth nanostructures. Nanoscale Res Lett. 2010;5(2):398–402.
29. Kumar Jena B, Retna Raj C. Gold nanoelectrode ensembles for the simultaneous electrochemical detection of ultratrace arsenic, mercury, and copper. Anal Chem. 2008;80 (13):4836–44.
30. Orozco J, Fernández-Sánchez C, Jiménez-Jorquera C. Underpotential deposition − anodic stripping voltammetric detection of copper at gold nanoparticle-modified ultramicroelectrode arrays. Environ Sci Technol. 2008;42(13):4877–82.
31. Gong J, Zhou T, Song D, Zhang L. Monodispersed Au nanoparticles decorated graphene as an enhanced sensing platform for ultrasensitive stripping voltammetric detection of mercury (II). Sensors Actuators B Chem. 2010;150(2):491–7.
32. Gong J, Zhou T, Song D, Zhang L, Hu X. Stripping voltammetric detection of mercury (II) based on a bimetallic Au− Pt inorganic− organic hybrid nanocomposite modified glassy carbon electrode. Anal Chem. 2009;82(2):567–73.
33. Renedo OD, Martínez MJA. A novel method for the anodic stripping voltammetry determination of Sb (III) using silver nanoparticle-modified screen-printed electrodes. Electrochem Commun. 2007;9(4):820–6.
34. Pan D, Wang Y, Chen Z, Lou T, Qin W. Nanomaterial/ionophore-based electrode for anodic stripping voltammetric determination of lead: an electrochemical sensing platform toward heavy metals. Anal Chem. 2009;81(12):5088–94.
35. Jang SH, Min BG, Jeong YG, Lyoo WS, Lee SC. Removal of lead ions in aqueous solution by hydroxyapatite/polyurethane composite foams. J Hazard Mater. 2008;152(3):1285–92.

36. Fu X-C, Chen X, Guo Z, Kong L-T, Wang J, Liu J-H, Huang X-J. Three-dimensional gold micro-/nanopore arrays containing 2-mercaptobenzothiazole molecular adapters allow sensitive and selective stripping voltammetric determination of trace mercury (II). Electrochim Acta. 2010;56(1):463–9.
37. Zhu Z, Su Y, Li J, Li D, Zhang J, Song S, Zhao Y, Li G, Fan C. Highly sensitive electrochemical sensor for mercury (II) ions by using a mercury-specific oligonucleotide probe and gold nanoparticle-based amplification. Anal Chem. 2009;81(18):7660–6.
38. Miao P, Liu L, Li Y, Li G. A novel electrochemical method to detect mercury (II) ions. Electrochem Commun. 2009;11(10):1904–7.
39. Kong R-M, Zhang X-B, Zhang L-L, Jin X-Y, Huan S-Y, Shen G-L, Yu R-Q. An ultrasensitive electrochemical "turn-on" label-free biosensor for Hg^{2+} with AuNP-functionalized reporter DNA as a signal amplifier. Chem Commun. 2009;37:5633–5.
40. Chianella I, Piletsky S, Tothill I, Chen B, Turner A. MIP-based solid phase extraction cartridges combined with MIP-based sensors for the detection of microcystin-LR. Biosens Bioelectron. 2003;18(2):119–27.
41. Thevenot DR, Toth K, Durst RA, Wilson GS. Electrochemical biosensors: recommended definitions and classification. Pure Appl Chem. 1999;71(12):2333–48.
42. Tothill IE. Biosensors developments and potential applications in the agricultural diagnosis sector. Comput Electron Agric. 2001;30(1):205–18.
43. Tothill IE. Biosensors for cancer markers diagnosis. Semi Cell Dev Biol. 2009; 20(1):55–62.
44. McNeil SE. Nanotechnology for the biologist. J Leukoc Biol. 2005;78(3):585–94.
45. Katz E, Willner I. Biomolecule-functionalized carbon nanotubes: applications in nanobioelectronics. ChemPhysChem. 2004;5(8):1084–104.
46. Katz E, Willner I, Wang J. Electroanalytical and bioelectroanalytical systems based on metal and semiconductor nanoparticles. Electroanalysis. 2004;16(12):19–44.
47. Willner I, Baron R, Willner B. Integrated nanoparticle–biomolecule systems for biosensing and bioelectronics. Biosens Bioelectron. 2007;22(9):1841–52.
48. Kerman K, Saito M, Tamiya E, Yamamura S, Takamura Y. Nanomaterial-based electrochemical biosensors for medical applications. TrAC Trends Anal Chem. 2008;27(7):585–92.
49. Wang J. Nanomaterial-based electrochemical biosensors. Analyst. 2005;130(4):421–6.
50. Logrieco A, Arrigan D, Brengel-Pesce K, Siciliano P, Tothill I. Microsystems technology solutions for rapid detection of toxigenic fungi and mycotoxins. Food Addit Contam. 2005;22:335–44.
51. Huang XJ, O'Mahony AM, Compton RG. Microelectrode arrays for electrochemistry: approaches to fabrication. Small. 2009;5(7):776–88.
52. Aguiar FA, Gallant A, Rosamond M, Rhodes A, Wood D, Kataky R. Conical recessed gold microelectrode arrays produced during photolithographic methods: characterisation and causes. Electrochem Commun. 2007;9(5):879–85.
53. Ordeig O, Godino N, del Campo J, Muñoz FX, Nikolajeff F, Nyholm L. On-chip electric field driven electrochemical detection using a poly (dimethylsiloxane) microchannel with gold microband electrodes. Anal Chem. 2008;80(10):3622–32.
54. Xu H, Malladi K, Wang C, Kulinsky L, Song M, Madou M. Carbon post-microarrays for glucose sensors. Biosens Bioelectron. 2008;23(11):1637–44.
55. Kress-Rogers E, Brimelow CJ. Instrumentation and sensors for the food industry. Cambridge: Woodhead Publishing; 2001.
56. Piermarini S, Micheli L, Ammida N, Palleschi G, Moscone D. Electrochemical immunosensor array using a 96-well screen-printed microplate for aflatoxin B 1 detection. Biosens Bioelectron. 2007;22(7):1434–40.
57. Ngundi MM, Shriver-Lake LC, Moore MH, Lassman ME, Ligler FS, Taitt CR. Array biosensor for detection of ochratoxin A in cereals and beverages. Anal Chem. 2005;77 (1):148–54.
58. Ngundi MM, Shriver-Lake LC, Moore MH, Ligler FS, Taitt CR. Multiplexed detection of mycotoxins in foods with a regenerable array. J Food Prot. 2006;69(12):3047–51.

59. van der Gaag B, Spath S, Dietrich H, Stigter E, Boonzaaijer G, van Osenbruggen T, Koopal K. Biosensors and multiple mycotoxin analysis. Food Control. 2003;14(4):251–4.
60. Ligler FS, Taitt CR, Shriver-Lake LC, Sapsford KE, Shubin Y, Golden JP. Array biosensor for detection of toxins. Anal Bioanal Chem. 2003;377(3):469–77.
61. Sapsford KE, Ngundi MM, Moore MH, Lassman ME, Shriver-Lake LC, Taitt CR, Ligler FS. Rapid detection of foodborne contaminants using an array biosensor. Sens Actuators B. 2006;113(2):599–607.
62. Parker CO, Lanyon YH, Manning M, Arrigan DW, Tothill IE. Electrochemical immunochip sensor for aflatoxin M1 detection. Anal Chem. 2009;81(13):5291–8.
63. Hafeman DG, Parce JW, Mcconnell HM. Light-addressable potentiometric sensor for biochemical systems. Science. 1988;240(4856):1182–5.
64. Owicki JC, Bousse LJ, Hafeman DG, Kirk GL, Olson JD, Wada HG, Parce JW. The light-addressable potentiometric sensor: principles and biological applications. Annu Rev Biophys Biomol Struct. 1994;23(23):87–113.
65. Hafner F. Cytosensor microphysiometer: technology and recent applications. Biosens Bioelectron. 2000;15(3–4):149–58.
66. Adami M, Sartore M, Nicolini C. PAB: a newly designed potentiometric alternating biosensor system. Biosens Bioelectron. 1995;10(95):155–67.
67. Liu Q, Yu H, Tan Z, Cai H, Ye W, Zhang M, Wang P. In vitro assessing the risk of drug-induced cardiotoxicity by embryonic stem cell-based biosensor. Sensors Actuators B Chem. 2011;155(1):214–9.
68. Wang P, Xu G, Qin L, Xu Y, Li Y, Li R. Cell-based biosensors and its application in biomedicine. Sensors Actuators B Chem. 2005;108(1–2):576–84.
69. Miller D. Cholinergic stimulation of the Na^+/K^+ adenosine triphosphatase as revealed by microphysiometry. Biophys J. 1993;64(3):813–23.
70. Xu G, Ye X, Qin L, Ying X, Yan L, Rong L, Ping W. Cell-based biosensors based on light-addressable potentiometric sensors for single cell monitoring. Biosens Bioelectron. 2005;20 (20):1757–63.
71. Cowey A, V.L.M. Instrumental biosensors: new perspectives for the analysis of biomolecular interactions. Bioessays 1999;21(4):339–52.
72. Eklund SE, Snider RM, Wikswo J, Baudenbacher F, Prokop A, Cliffel DE. Multianalyte microphysiometry as a tool in metabolomics and systems biology. J Electroanal Chem. 2006;587(2):333–9.
73. Eklund SE, Thompson RG, Snider RM, Carney CK, Wright DW, John W, Cliffel DE. Metabolic discrimination of select list agents by monitoring cellular responses in a multianalyte microphysiometer. Sensors. 2009;9(3):2117–33.
74. Mcconnell HM, Owicki JC, Parce JW, Miller DL, Baxter GT, Wada HG, Pitchford S. The cytosensor microphysiometer: biological applications of silicon technology. Science. 1992;257(5078):1906–12.
75. Garnovskaya MN, Mukhin YV, Vlasova TM, Raymond JR. Hypertonicity activates $Na^{+/}H^+$ exchange through Janus kinase 2 and calmodulin. J Biol Chem. 2003;278(19):16908–15.
76. Ellis AG, Doherty MM, Walker F, Weinstock J, Nerrie M, Vitali A, Murphy R, Johns TG, Scott AM, Levitzki A. Preclinical analysis of the analinoquinazoline AG1478, a specific small molecule inhibitor of EGF receptor tyrosine kinase. Biochem Pharmacol. 2006;71 (10):1422–34.
77. Okada Y, Taniguchi T, Akagi Y, Muramatsu I. Two-phase response of acid extrusion triggered by purinoceptor in Chinese hamster ovary cells. Eur J Pharmacol. 2002;455 (1):19–25.
78. Fujii R, Hosoya M, Fukusumi S, Kawamata Y, Habata Y, Hinuma S, Onda H, Nishimura O, Fujino M. Identification of neuromedin U as the cognate ligand of the orphan G protein-coupled receptor FM-3. J Biol Chem. 2000;275(28):21068–74.

79. Kramarenko I, Bunni M, Morinelli TA, Raymond J, Garnovskaya M. Identification of functional bradykinin B(2) receptors endogenously expressed in HEK293 cells'. Biochem Pharmacol. 2009;77(77):269–76.
80. Coaxum SD, Garnovskaya MM. Epidermal growth factor activates Na(+/)H(+) exchanger in podocytes through a mechanism that involves Janus kinase and calmodulin. Biochim Biophys Acta. 2009;1793(7):1174–81.
81. Gonzalo A, Tze-Jen H, Catherine W, Alex V, Paul F, Gibson RM. Insulin-like growth factor-1-dependent maintenance of neuronal metabolism through the phosphatidylinositol 3-kinase-Akt pathway is inhibited by C2-ceramide in CAD cells. Eur J Neurosci. 2007;25(10):3030–8.
82. Fischer H, Seelig A, Beier N, Raddatz P, Seelig J. New drugs for the Na^+/H^+ exchanger. Influence of Na^+ concentration and determination of inhibition constants with a microphysiometer. J Membr Biol. 1999;168(1):39–45.
83. V.X.D.O. Jr, Fázio MA, Santos EL, Pesquero JB, Miranda A. In vitro evaluation of leptin fragments activity on the ob receptor. J Pept Sci Off Publ Eur Pept Soc. 2008;14(5):617–25.
84. Douglas ES, Hsiao SC, Onoe H, Bertozzi CR, Francis MB, Mathies RA. DNA-barcode directed capture and electrochemical metabolic analysis of single mammalian cells on a microelectrode array. Lab Chip. 2009;9(14):2010–5.
85. Cunha FM, Berti DA, Ferreira ZS, Klitzke CF, Markus RP, Ferro ES. Intracellular peptides as natural regulators of cell signaling. J Biol Chem. 2008;283(36):24448–59.
86. Santos EL, Reis RI, Silva RG, Shimuta SI, Pecher C, Bascands JL, Schanstra JP, Oliveira L, Bader M, Paiva ACM. Functional rescue of a defective angiotensin II AT1 receptor mutant by the Mas protooncogene. Regul Pept. 2007;141(1–3):159–67.
87. Santos EL, Souza KDP, Sabatini RA, Martin RP, Fernandes L, Nardi DT, Malavolta L, Shimuta SI, Nakaie CR, Pesquero JB. Functional assessment of angiotensin II and bradykinin analogues containing the paramagnetic amino acid TOAC. Int Immunopharmacol. 2008;8 (2):293–9.
88. Karin B, Lena P, Kjell L. Metabolic activation of A549 human airway epithelial cells by organic dust: a study based on microphysiometry. Life Sci. 2002;71(3):299–309.
89. Belgin S, Ismail B, Ahmet G, Khan O. Functional analysis of amino acids of the Na^+/H^+ exchanger that are important for proton translocation. Mol Cell Biochem. 2003;254 (1–2):117–24.
90. Smart D, Wood MD. Cytosensor techniques for examining signal transduction of neurohormones. Biochem Cell Biol. 2000;78(78):281–8.
91. Roth C, Kohen R, Walton S, Yarmush M. Coupling of inflammatory cytokine signaling pathways probed by measurements of extracellular acidification rate. Biophys Chem. 2001;89(1):1–12.
92. Parce JW, Owicki JC, Kercso KM, Sigal GB, Wada HG, Muir VC, Bousse LJ, Ross KL, Sikic BI, Mcconnell HM. Detection of cell-affecting agents with a silicon biosensor. Science. 1989;246(4927):243–7.
93. Bruner LH, Miller KR, Owicki JC, Parce JW, Muir VC. Testing ocular irritancy in vitro with the silicon microphysiometer. Toxicol In Vitro Int J Publ Assoc Bibra. 1991;5(4):277–84.
94. Landin W, Mun G, Nims R, Harbell J. Use of the cytosensor microphysiometer to predict results of a 21-day cumulative irritation patch test in humans. Toxicol In Vitro. 2007;21 (6):1165–73.
95. Waldenmaier DS, Babarina A, Kischkel FC. Rapid in vitro chemosensitivity analysis of human colon tumor cell lines. Toxicol Appl Pharmacol. 2003;192(3):237–45.
96. Yicong W, Ping W, Xuesong Y, Qingtao Z, Rong L, Weimin Y, Xiaoxiang Z. A novel microphysiometer based on MLAPS for drugs screening. Biosens Bioelectron. 2001;16 (4–5):277–86.
97. Wu Y, Wang P, Ye X, Zhang G, He H, Yan W, Zheng X, Han J, Cui D. Drug evaluations using a novel microphysiometer based on cell-based biosensors. Sensors Actuators B Chem. 2001;80(3):215–21.

98. Siqueira JR, Werner CF, Bäcker M, Poghossian A, Zucolotto V, Oliveira ON, Schöning MJ. Layer-by-layer assembly of carbon nanotubes incorporated in light-addressable potentiometric sensors. J Phys Chem. 2009;113(33):14765–70.
99. Ismail ABM, Yoshinobu T, Iwasaki H, Sugihara H, Yukimasa T, Hirata I, Iwata H. Investigation on light-addressable potentiometric sensor as a possible cell-semiconductor hybrid. Biosens Bioelectron. 2003;18(12):1509–14.
100. Stein B, George M, Gaub HE, Parak WJ. Extracellular measurements of averaged ionic currents with the light-addressable potentiometric sensor (LAPS). Sensors Actuators B Chem. 2004;98(2):299–304.
101. Liu Q, Cai H, Xu Y, Li Y, Li R, Wang P. Olfactory cell-based biosensor: a first step towards a neurochip of bioelectronic nose. Biosens Bioelectron. 2006;22(2):318–22.
102. George M, Parak WJ, Gerhardt I, Moritz W, Kaesen F, Geiger H, Eisele I, Gaub HE. Can the light-addressable potentiometric sensor (LAPS) detect extracellular potentials of cardiac myocytes? Sensors Actuators A Phys. 2000;47(8):1106–13.
103. Zhang W, Li Y, Liu Q, Xu Y, Cai H, Wang P. A novel experimental research based on taste cell chips for taste transduction mechanism. Sensors Actuators B Chem. 2008;131(1):24–8.
104. George M, Parak WJ, Gaub HE. Highly integrated surface potential sensors. Sensors Actuators B Chem. 2000;69(3):266–75.
105. Liu Q, Cai H, Xu Y, Xiao L, Yang M, Wang P. Detection of heavy metal toxicity using cardiac cell-based biosensor. Biosens Bioelectron. 2007;22(12):3224–9.
106. Liu Q, Cai H, Xiao L, Li R, Yang M, Wang P. Embryonic stem cells biosensor and its application in drug analysis and toxin detection. Sensors J IEEE. 2007;7(12):1625–31.
107. Liu Q, Ye W, Yu H, Hu N, Du L, Wang P, Yang M. Olfactory mucosa tissue-based biosensor: a bioelectronic nose with receptor cells in intact olfactory epithelium. Sensors Actuators B Chem. 2010;146(2):527–33.
108. Bucher V, Leibrock C, Schubert MNW, Brunner B. Electrical properties of a light-addressable microelectrode chip with high electrode density for extracellular stimulation and recording of excitable cells. Biosens Bioelectron. 2001;16(3):205–10.
109. Artem S, Jung C, Sebastian HS. Light-directed electrical stimulation of neurons cultured on silicon wafers. J Neurophysiol. 2005;93(2):1090–8.